Control of the Orbital Delocalization and Implications for Molecular Rectification in the Radical Anions of Porphyrins with Coplanar 90° and 180° β,β′-Fused Extensions

Wenbo E,[†] Karl M. Kadish,*[,†] Paul J. Sintic,[‡] Tony Khoury,[‡] Linda J. Govenlock,[‡] Zhongping Ou,[†] Jianguo Shao,[†] Kei Ohkubo,[§] Jeffrey R. Reimers,[‡] Shunichi Fukuzumi,*[,§] and Maxwell J. Crossley*[,‡]

Department of Chemistry, University of Houston, Houston, Texas 77204-5003, School of Chemistry, The University of Sydney, NSW 2006, Australia, and Department of Material and Life Science, Graduate School of Engineering, Osaka University, SORST, Japan Science and Technology Agency, Suita, Osaka 565-0871, Japan

Received: August 9, 2007; In Final Form: October 11, 2007

Through-porphyrin electronic communication is investigated using "linear-type" and "corner-type" bis-(quinoxalino)porphyrins in free-base form and their Zn^{II}, Cu^{II}, Ni^{II}, and Pd^{II} derivatives. These compounds are porphyrins with quinoxalines fused on opposite or adjacent β,β′-pyrrolic positions; they were synthesized from 5,10,15,20-tetrakis(3,5-di-*tert*-butylphenyl)-porphyrin-2,3,12,13- and -2,3,7,8-tetraone, respectively, by reaction with 1,2-phenylenediamine. The degree of electron spin delocalization into the fused rings in the π-radical anions of the free-base and metal(II) bisquinoxalinoporphyrins was elucidated by electrochemistry, UV−vis absorption, and electron spin resonance (ESR) spectra of the singly reduced species and density functional theory calculations. Hyperfine splitting patterns in the ESR spectra of the π-radical anions show that symmetric molecules have delocalized electron spin, indicating that significant inter-quinoxaline interactions are mediated through the central porphyrin unit, these interactions being sufficient to guarantee through-molecule conduction. However, when molecular symmetry is broken by tautomeric exchange of the inner nitrogen hydrogens in the free-base porphyrin with a corner-type quinoxaline substitution pattern, the π-radical anion becomes confined so that one quinoxaline group is omitted from spin delocalization. This indicates the appearance of a unidirectional barrier to through-molecule conduction, suggesting a new motif for chemically controlled rectification.

Introduction

Metalloporphyrins and their derivatives have attracted much interest with respect to their applications in the area of functional molecular devices.[1−6] Much of the interest in these compounds derives from their structural homology and similar redox properties to macrocycles found in biological systems, which are responsible for life-sustaining processes such as long-range electron transfer and the transport of oxygen.[7−9] Indeed, the charge-separation and electron-conduction properties of the photosynthetic reaction center (PRC) establish the paradigm for "molecular electronics" and the concept of "molecular wires". The PRC and the associated light-harvesting systems consist of arrays of porphinoid compounds at the porphyrin, chlorin (dihydroporphyrin), bacteriochlorin, and isobacteriochlorin (tetrahydroporphyrin) levels of oxidation, depending on the organism and role being played by the particular chromphore.[10] In these systems, the chromophores are held fairly rigidly but in a variety of relative orientations between successive units, depending on where they are in the chain of events. The relative orientations and interchromophore distances presumably have evolved to maximize energy capture and transfer, transduction of the energy to charge, or conduction of electrons away from the PRC. These arrays are self-assembled systems and so do not involve covalent linkages between adjacent components, the architecture being established and maintained by an apoprotein matrix with specific sites for binding the chromophores. Interchromophore communication therefore essentially involves through-space interactions.

Synthetic analogues of these "molecular electronic" natural systems have been constructed but without the apoprotein matrix, and therefore, they necessarily have covalent linkages between the chromophores to maintain the molecular architecture.[2,6,11,12] As a consequence, the extent of coupling between the chromophores in synthetic systems will be in part dependent on the nature of the molecular linkages as through-bond communication becomes a possibility.[4] Many different architectures can result, depending on the position or region of the porphyrin nucleus that is elaborated. Meso- and β-positions of the macrocycle have been used as attachment points,[13−15] and β,β′-pyrrolic,[16,17] β,meso,[18] and β,meso,β faces[19] have been regions for fusion of annulated rings (Figure 1). In addition, extension into the third dimension is possible through chelation to coordinated metal ions.

Arrays have been reported in which porphyrins are laterally extended in a linear fashion from opposite sides on the periphery, with the ultimate goal being their utilization as molecular wires.[20−23] The electronic communication in synthetic porphyrin systems that are electronically coupled through bonds, in principle, can be modified or switched. Such switching has been demonstrated in a linear coplanar bis-porphyrin that incorporated

* Authors to whom correspondence should be addressed. E-mail: kkadish@uh.edu; fukuzumi@chem.eng.osaka-u.ac.jp; m.crossley@chem.usyd.edu.au.
[†] University of Houston.
[‡] The University of Sydney.
[§] Osaka University.

10.1021/jp076406g CCC: $40.75
Published on Web 01/03/2008

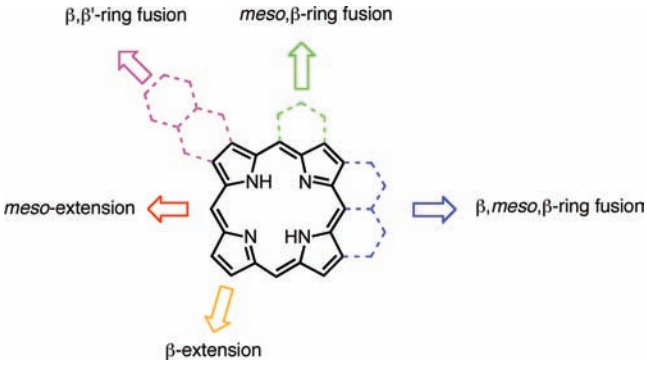

Figure 1. Positions for ring extension and ring fusion on the porphyrin periphery.

a quinonoid unit that could be modified by both redox and chemical means.[24] Few systems have been prepared that incorporate multidirectionality,[25−27] a concept that might be important for high-density architectures and for use in gating mechanisms.[28−30] The well-known chemistry at the β-pyrrolic periphery of a porphyrin macrocycle provides the necessary synthetic control to allow for multidirectional extension,[27,31] an example of which is shown in Figure 2 where both linear and 90° geometries are included to create a proposed array. Also highlighted in this figure are the key molecular components, where two quinoxaline groups are fused to the porphyrin macrocycle in either a linear or a corner fashion.

In this paper, electronic communication through the porphyrin ring is investigated by focusing on these bisquinoxalinoporphyrin molecular arrangements. The structures of the newly investigated macrocycles are shown in Chart 1 and are given the notation (QPQ)M **3** for the "linear" bisquinoxalinoporphyrins and (PQ_2)M **4** for the "corner" bisquinoxalinoporphyrins (M = 2H, Zn^{II}, Cu^{II}, Ni^{II}, or Pd^{II}).[32]

The doubly ring-annulated bisquinoxalinoporphyrins (QPQ)M (**3**) and (PQ_2)M (**4**) are quite valuable in that an investigation of their fundamental electronic properties, in particular the degree of communication between two quinoxaline units upon electron transfer, should provide insight into the functionality and potential applications of these molecules when used as components in molecular wires. The (QPQ)M (**3**) component has already been shown to facilitate electron transfer through a super-exchange mechanism in giant multiporphyrin arrays that were designed as close distance and orientation models of the PRC.[12,33] Therefore, an understanding of the electronic properties of (QPQ)M (**3**) and (PQ_2)M (**4**) upon one-electron reduction is desirable. In particular, a knowledge of the degree of spin distribution on the two fused quinoxaline units is important to control the electron coupling term in porphyrin-based molecular wires that might contain these components. Herein we report how the extent of communication between the two quinoxaline units in a bisquinoxalinoporphyrin can be controlled by changes in either the nature of the central substitution (protons versus metal(II) ion) in conjunction with the geometry of the two fused quinoxaline groups, being opposite to each other in one case and at adjacent sites of the porphyrin in the other. Electrochemical and UV−vis spectroelectrochemical techniques are used to ascertain the electronic character and possible applications of these systems. The present study provides valuable insight into the rational design of porphyrin-based molecular wires for applications as chemically controlled molecular conductors and rectifiers.

Results and Discussion

Synthesis of Bisquinoxalinoporphyrins. The bisquinoxalinoporphyrins were prepared by the reaction of porphyrin-tetraones with 1,2-phenylenediamine (**6**). Linear bisquinoxalinoporphyrin (QPQ)2H (**3a**) was readily prepared in 95% yield by reaction of linear tetraone **5**[27] with an excess of 1,2-phenylenediamine **6** (Scheme 1a). (QPQ)2H (**3a**) has a D_{2h} element of symmetry that is clearly evident by the signal pattern in the ^{1}H NMR spectrum. The spectrum contained a 72-proton doublet for the *tert*-butyl protons, a four-proton triplet and an eight-proton doublet for the aryl protons of the meso phenyl rings, and a downfield four-proton doublet due to the β-pyrrole protons. This doublet collapsed to a singlet upon irradiation of the broad singlet upfield of tetramethylsilane due to the loss of the ^4J coupling to the inner NH protons. This indicates that the aromatic pathway in this molecule is essentially locked in the tautomer as drawn in Figure 3a, where the inner NH protons reside on the non-annulated pyrrolic rings.[33] This confirms that (QPQ)2H (**3a**) has a bacteriochlorin-like aromatic pathway. The UV−vis spectrum of (QPQ)2H (**3a**) shows a broad red-shifted Soret band (449 nm (log ϵ = 5.41)) and Q-bands that tail to higher wavelengths when compared to non-annulated porphyrins.

Likewise, corner bisquinoxalinoporphyrin (PQ_2)2H (**4a**) was readily prepared in 94% yield by the condensation of corner tetraone **7** and 1,2-phenylenediamine **6** (Scheme 1b). The ^{1}H NMR spectrum of (PQ_2)2H (**4a**) shows a C_{2v} symmetry pattern in which *tert*-butyl protons and aryl protons on the meso ring all give rise to signals in a 1:2:1 ratio, respectively, and the four β-pyrrolic protons appear as a downfield AB quartet. The C_{2v} symmetry pattern in the ^{1}H NMR spectrum of (PQ_2)2H (**4a**) is an indication that the inner NH protons of the porphyrinoid ring are in fast exchange on the NMR time scale, and this is supported by the lack of resolved ^4J coupling between the β-pyrrolic and the inner NH protons, confirming the isobacteriochlorin-like character of (PQ_2)2H (**4a**). In fact, the inner NH protons have experienced a downfield shift as a result of the lowering aromaticity associated with the isobacteriochlorin ring structure and appear as a broad singlet at −0.55 ppm. At low temperature (220 K) in $CDCl_3$, this broad singlet begins to split in the ^{1}H NMR spectrum as the exchange process becomes observable on the NMR time scale, and the inequivalence of the inner NH protons of (PQ_2)2H (**4a**) becomes apparent. This indicates that the aromatic delocalization pathway in this molecule alternates between two degenerate forms as shown in Figure 3b with any given $\beta-\beta$ bond in (PQ_2)2H (**4a**) being alternately aromatic or ethylenic depending on which tautomer is present.[34]

The metalation properties of (QPQ)2H (**3a**) and (PQ_2)2H (**4a**) were investigated by heating a solution of the porphyrin with the appropriate metal salt in a suitable solvent mixture that enhanced the solubility of reagents (Scheme 1). It was found that (PQ_2)2H (**4a**) was much easier to metalate than its linear isomer, (QPQ)2H (**3a**); for example, quantitative zinc(II) chelation of (PQ_2)2H (**4a**) was achieved by heating at reflux a mixture of a chloroform−methanol (2:1) solution of the porphyrin and zinc(II) acetate dihydrate for 3 min, whereas 18 h were required to complete the metalation of (QPQ)2H (**4a**) under identical conditions. Using conditions recently reported for the metalation of linear and corner porphyrin-tetraones,[31] the other metalations of (QPQ)2H (**3a**) and (PQ_2)2H (**4a**) were achieved in almost quantitative yield. The general UV−vis spectral patterns for (QPQ)M (**3**) and (PQ_2)M (**4**) resemble those of other compounds with bacteriochlorin and isobacteriochlorin

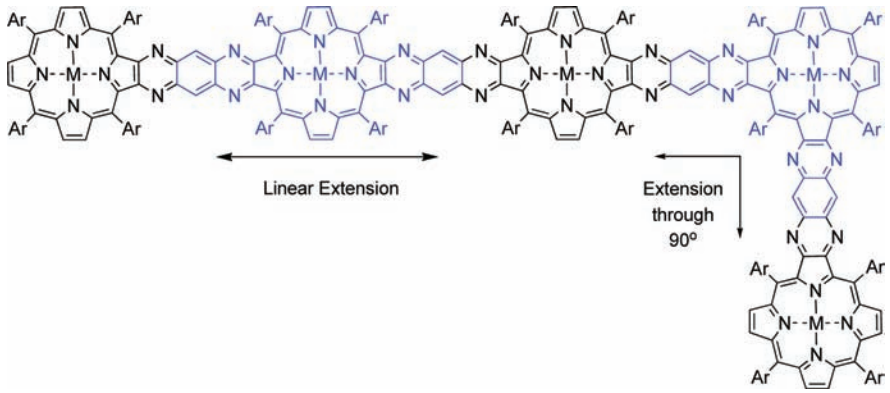

Figure 2. Proposed molecular wire with linear and corner bisquinoxalinoporphyrin components colored in blue (Ar = 3,5-di-*tert*-butylphenyl).

CHART 1

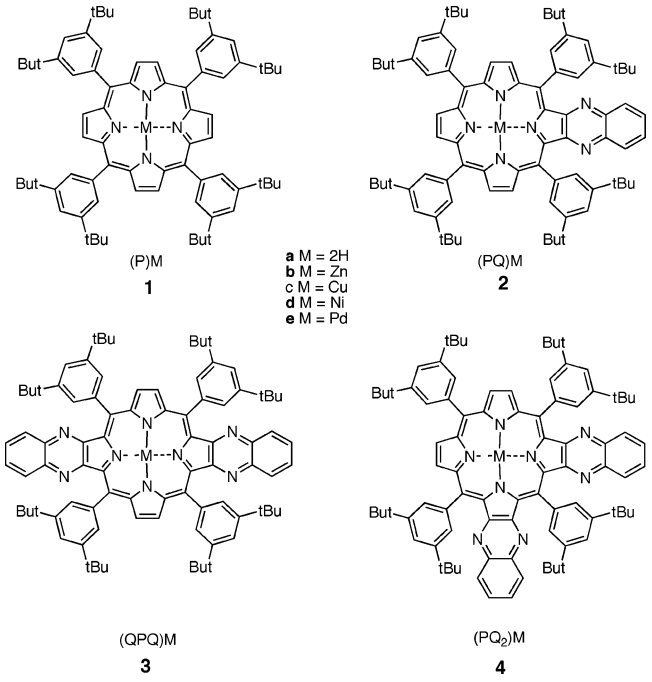

structures, respectively.[35,36] In the case of (QPQ)M (**3b**−**e**), the Soret bands are split and shifted toward the red, and there is an increase in the lower-energy Q-band intensities. For (PQ_2)M (**4b**−**e**), λ_{max} occurs near 420 nm, and the Q-bands are tailed to higher wavelengths. Unlike the free-base analogues, the metallo-bisquinoxalinoporphyrins (QPQ)M (**3b**−**e**) and (PQ_2)M (**4b**−**e**) cannot exist in equilibrating tautomeric forms.[37]

These optimized metalation conditions for (QPQ)2H (**3a**) and (PQ_2)2H (**4a**) provide increased synthetic flexibility in preparing functional multiporphyrin arrays, which will enable further redox manipulation in complex β-pyrrolic fused arrays by having more control of the desired synthetic objectives (vide infra).

Electrochemistry of Free-Base and Metalated Bisquinoxalinoporphyrins. Cyclic voltammograms of the mono- and bisquinoxalinoporphyrins (PQ)2H (**2a**), (QPQ)2H (**3a)**, and (PQ_2)2H (**4a)** in CH_2Cl_2 containing 0.1 M tetra-*n*-butylammonium perchlorate (TBAP) are shown in Figure 4. The $E_{1/2}$ for the first reduction of (QPQ)2H (**3a**) is positively shifted by 100 mV from $E_{1/2}$ for the first reduction of (PQ)2H (**2a**). A larger $\Delta E_{1/2}$ value is obtained between reduction of (PQ)2H (**2a**) and (PQ_2)2H (**4a**) (160 mV), while at the same time the irreversible oxidations of (QPQ)2H (**3a**) (E_p = 1.02 V) and (PQ_2)2H (**4a**) (E_p = 1.00 V) are located at almost the same potential as that for the reversible oxidation of (PQ)2H (**2a**) (for a scan rate of 0.10 V/s). The latter result indicates that fusion of a second quinoxaline group onto (PQ)2H (**2a**) has little or no effect on the highest occupied molecular orbitals (HOMOs) of the free-base bisquinoxalinoporphyrins.

Figure 5 illustrates cyclic voltammograms for Zn(II) complexes of the related mono- and bisquinoxalinoporphyrins (PQ)Zn (**2b**), (PQ_2)Zn (**4b**), and (QPQ)Zn (**3b**) in CH_2Cl_2 containing 0.10 M TBAP. Also shown in this figure is a cyclic voltammogram of (P)Zn (**1b**) obtained under the same conditions. As seen in the figure, the reversible potential for the first oxidation of (PQ)Zn (**2b**; $E_{1/2}$ = 0.72 V) is the same as that of (P)Zn (**1b**; $E_{1/2}$ = 0.72 V). This indicates that fusion of a quinoxaline group onto the porphyrin ring has no effect on the HOMO of (PQ)Zn. The first reversible oxidation potentials of (PQ_2)Zn (**4b**) and (QPQ)Zn (**3b**) are positively shifted by only 50 and 40 mV, respectively, as compared with that of (PQ)Zn (**2b**). Thus, fusion of a second quinoxaline group onto (PQ)Zn has a small effect on the HOMO of zinc bisquinoxalinoporphyrins as is the case for free-base bisquinoxalinoporphyrins. As shown in Table 1, the $E_{1/2}$ values for the first oxidation of other metalated compounds (QPQ)M (**3a**−**e**) and (PQ_2)M (**4a**−**e**) with the same metal ion are also identical within experimental error; i.e., the difference in potentials between the two series of compounds with the same metal ions is only 10−20 mV.

In contrast to the first oxidation, the reversible potential for the first reduction of (QPQ)Zn (**3b**) in CH_2Cl_2 ($E_{1/2}$ = −1.14 V) is positively shifted by 170 mV from the $E_{1/2}$ for the first one-electron reduction of (PQ)Zn (**2b**) in the same solvent. This difference in reduction potentials between (PQ)Zn and (QPQ)Zn also contrasts with what is observed for the free-base derivatives with the same macrocycle, i.e., between (PQ)2H (**2a**) and (QPQ)2H (**3a**) where the difference in $E_{1/2}$ amounts to only 100 mV as seen in Figure 4. However, the positive shift in $E_{1/2}$ for the first reduction of (PQ_2)Zn (**4b**) is only 20 mV from (PQ)Zn (**2b**), whereas the positive shift for the corresponding free-base derivatives is 160 mV (Figure 4). Thus, there is a significant difference between the free-base and metal(II) bisquinoxalinoporphyrins upon one-electron reduction, as highlighted above and shown in Table 1 for other metal(II) derivatives.

Similar differences in $E_{1/2}$ for the one-electron reduction of the mono- and bisquinoxalinoporphyrins are observed for the other metalated compounds in CH_2Cl_2 (Table 1). The "linear-type" bisquinoxalinoporphyrins, (QPQ)M (**3**), are in all cases easier to reduce by 120−200 mV as compared to the (PQ)M (**2**) derivatives with the same central metal ions, while the "corner-type" bisquinoxalinoporphyrins, (PQ_2)M (**4**), are easier to reduce by only 20−60 mV as compared to (PQ)M (**2**) (Table 1). Also, as seen in Table 1, (QPQ)Cu (**3c**) and (QPQ)Pd (**3e**) undergo two reversible and well-separated one-electron oxida-

SCHEME 1 [a]

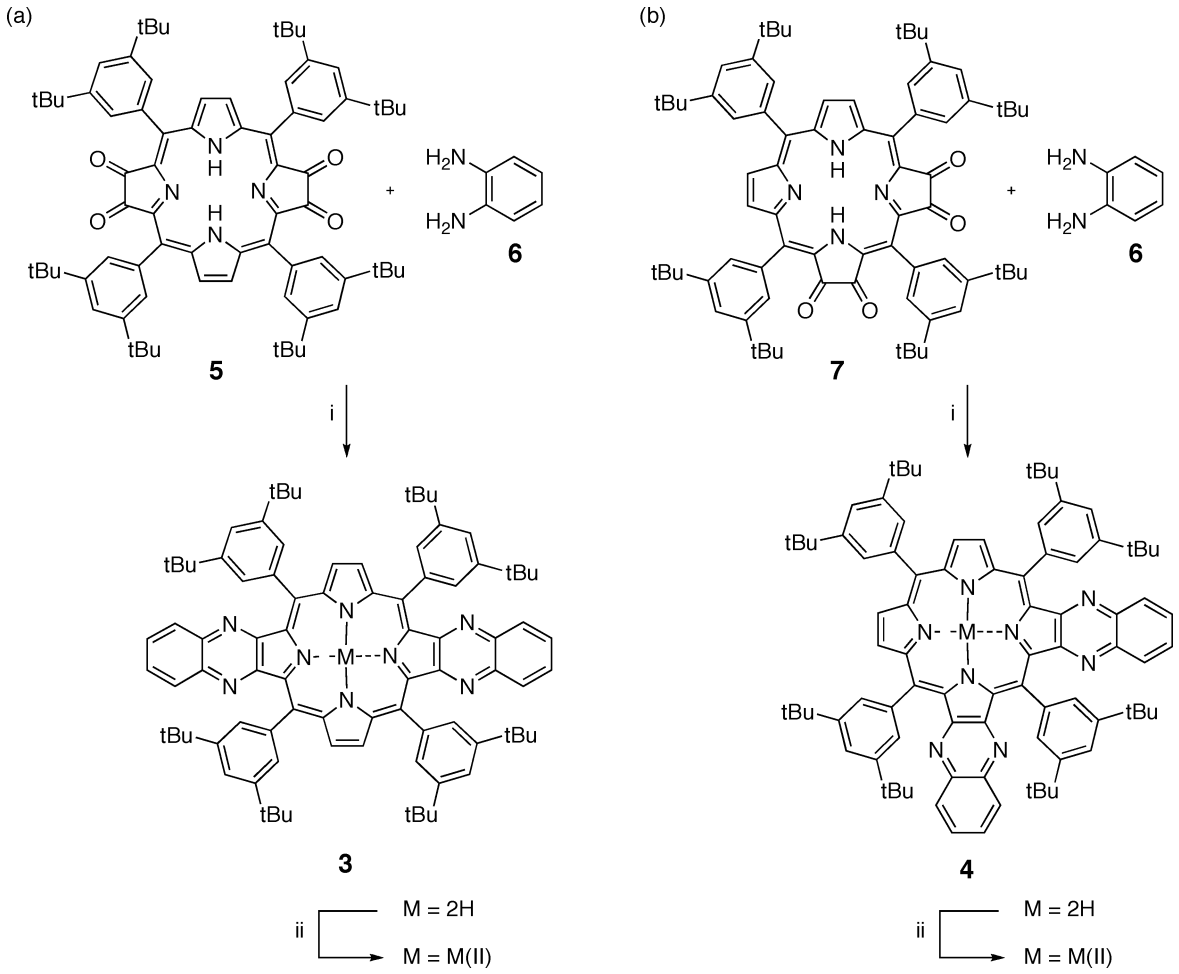

[a] Reagents and conditions: i, $CHCl_3$, stir; ii, conditions for metal chelation as described in the Experimental section.

tions to stepwise give π-cation radicals and dications, but these ring-centered oxidations are overlapped in potential for (QPQ)-Ni (**3d**), thus giving an overall two-electron conversion of the initial compound to what is most likely a porphyrin π-dication. Overlapped oxidations have been reported for a number of Ni-(II) porphyrins with other macrocycles,[39,40] and this behavior is not specific to the Ni(II) bisquinoxalinoporphyrin complexes.

HOMO−LUMO Gap. A summary of the experimentally measured HOMO−LUMO gaps of the different metal(II) bisquinoxalinoporphyrins in CH_2Cl_2 is given in Table 1 along with the measured values for (PQ)M (**2**). The HOMO−LUMO gaps for the free-base derivatives were not quoted as the first oxidations were irreversible and distorted by a chemical reaction. These gaps are listed as $\Delta E_{1/2}$ in Table 1 and decrease in the following order: (PQ)M (**2**) > (PQ_2)M (**4**) > (QPQ)M (**3**) for complexes with the same central metal ion. This result reflects mainly the change in the lowest unoccupied molecular orbital (LUMO) energy because the HOMO energy remains nearly the same in this series. Addition of a second quinoxaline group to (PQ)M (**2**) at an adjacent β-pyrrolic site to give (PQ_2)M (**4**) has only a minor effect on the electrochemistry of the porphyrin macrocycle. In contrast, the significant decrease of the HOMO−LUMO gap upon going from (PQ)M (**2**) to (QPQ)M (**3**) (on the order of 200 mV) can be accounted for by a stabilization of the porphyrin LUMO upon addition of the second fused quinoxaline group and also indicates that placement of the two quinoxaline groups in a linear fashion will have a profound effect on reduction potentials.

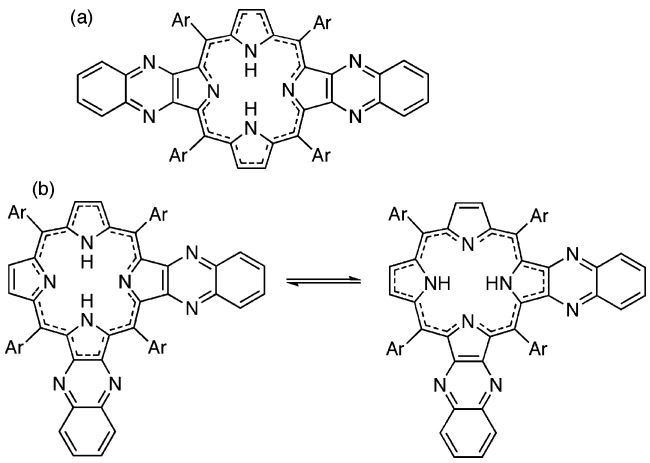

Figure 3. Aromatic delocalization pathway in (a) (QPQ)2H (**3a**), which is essentially locked in a single tautomer, and (b) (PQ_2)2H (**4a**) where the tautomers are degenerate and rapidly interconvert (Ar = 3,5-di-*tert*-butylphenyl).

UV−Vis Spectroelectrochemistry. The UV−vis spectral changes obtained during reduction of (QPQ)2H (**3a**) and (PQ_2)-2H (**4a**) in a thin-layer cell are shown in Figure 6. The broad absorption band at 700−800 nm and the disappearance of the Q-bands at 500−700 nm upon addition of one electron are both consistent with formation of a porphyrin π-radical anion. In the case of (PQ_2)2H (**4a**), the diagnostic porphyrin π-radical anion band is split into two absorption maxima at 740 and 786 nm, and this can be accounted for by a lowering of symmetry from

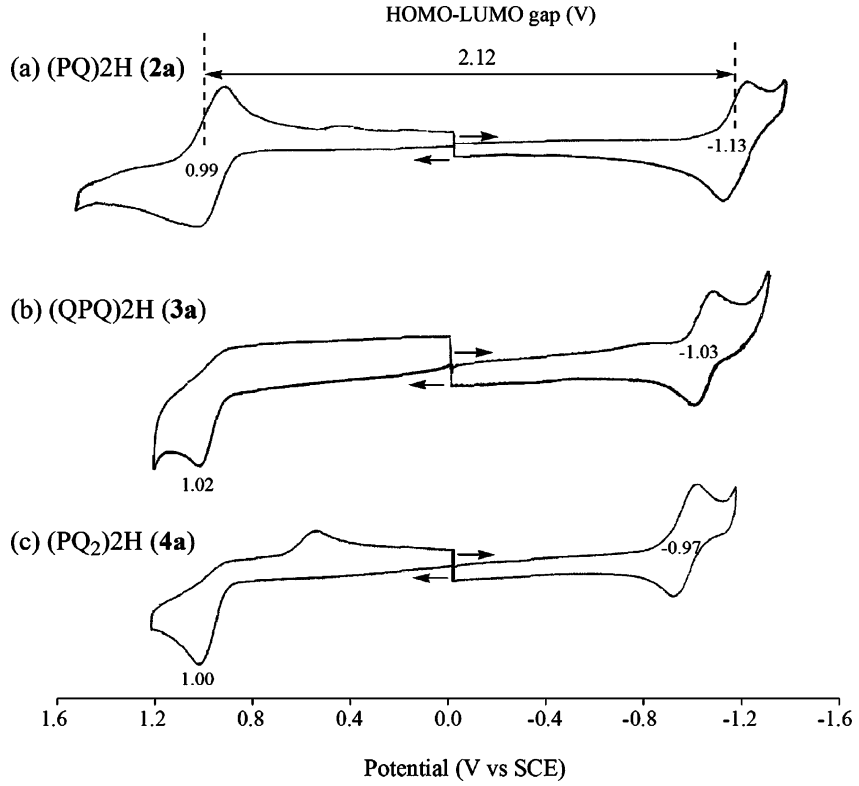

Figure 4. Cyclic voltammograms of (a) (PQ)2H (**2a**), (b) (QPQ)2H (**3a**), and (c) $(PQ_2)2H$ (**4a**) free-base compounds in CH_2Cl_2, 0.1 M TBAP.

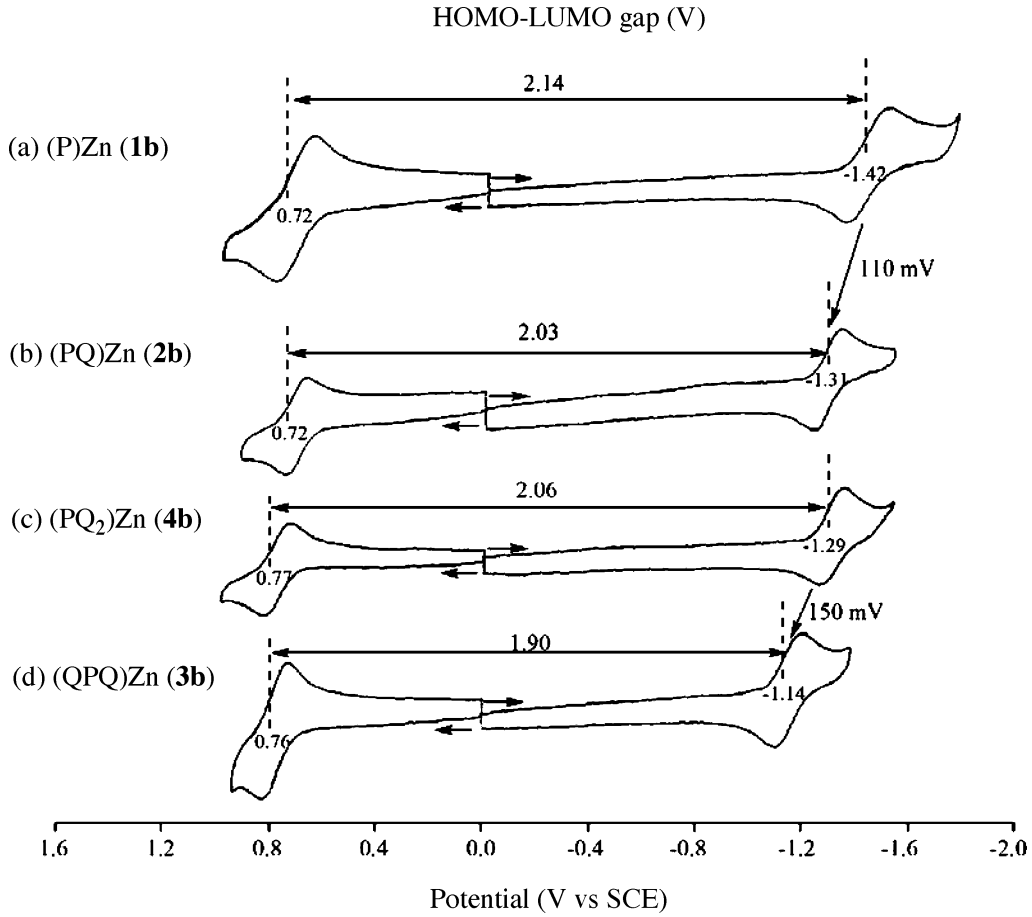

Figure 5. Cyclic voltammograms of (a) (P)Zn (**1b**), (b) (PQ)Zn (**2b**), (c) $(PQ_2)Zn$ (**4b**), and (d) (QPQ)Zn (**3b**) in CH_2Cl_2, 0.1 M TBAP.

D_{2h} for **3a** to C_{2v} for **4a**. UV−vis spectra for radical anions of the metalated derivatives also exhibit an absorption band that can be assigned to the porphyrin π-radical anion. Typical examples of these spectra are shown in Figure 7 for (QPQ)Cu (**3c**) and (PQ)Cu (**2c**), respectively. The λ_{max} value of the linear bisquinoxalinoporphyrin (QPQ)Cu (**3c**) radical anion (760 nm)

TABLE 1: Half-Wave or Peak Potentials (V vs SCE) and HOMO−LUMO Gap (ΔE_1) of (PQ)M (2), (QPQ)M (3), and (PQ_2)M (4) in CH_2Cl_2 Containing 0.1 M TBAP

		oxidation[a]			reduction			
	M	second	first	ΔE_1 (V)	first	second	third	fourth
PQ (**2**)[c]	2H		0.99 (1e)	2.12	−1.13	−1.33		
	Zn^{II}	1.10[d] (1e)	0.72 (1e)	2.03	−1.31	−1.75[d]		
	Cu^{II}	1.30[d] (1e)	0.97 (1e)	2.16	−1.19	−1.72[d]		
	Ni^{II}		0.95 (2e)	2.07	−1.12	−1.59[d]		
	Pd^{II}	1.46[d] (1e)	1.06 (1e)	2.22	−1.16	−1.62[d]		
QPQ (**3**)	2H		1.02[d] (1e)		−1.03	−1.32[d]		
	Zn^{II}	0.93 (1e)	0.76 (1e)	1.90	−1.14	−1.42		
	Cu^{II}	1.04 (1e)	0.91 (1e)	1.90	−0.99	−1.40		
	Ni^{II}		0.92 (2e)	1.92	−1.00	−1.40		
	Pd^{II}	1.41 (1e)	1.01 (1e)	2.01	−1.00	−1.43		
PQ_2 (**4**)	2H		1.00[d] (1e)		−0.97	−1.23	−1.60[d]	−1.78[d]
	Zn^{II}	1.08[d] (1e)	0.77 (1e)	2.06	−1.29	−1.58[d]	−1.73[d]	−1.91[d]
	Cu^{II}	1.03 (1e)	0.92 (1e)	2.05	−1.13	−1.58[d]	−1.68[d]	−1.96[d]
	Ni^{II}		0.93 (2e)	2.00	−1.07	−1.64[d]	−1.76[d]	
	Pd^{II}	1.38 (1e)	0.99 (1e)	2.13	−1.14	−1.56[d]	−1.66[d]	−1.90[d]

[a] Numbers of transferred electrons are given in parentheses. [b] ΔE_1 is the electrochemical HOMO−LUMO gap. [c] Taken from ref 38. [d] Peak potential at a scan rate of 0.1 V/s for irreversible reaction.

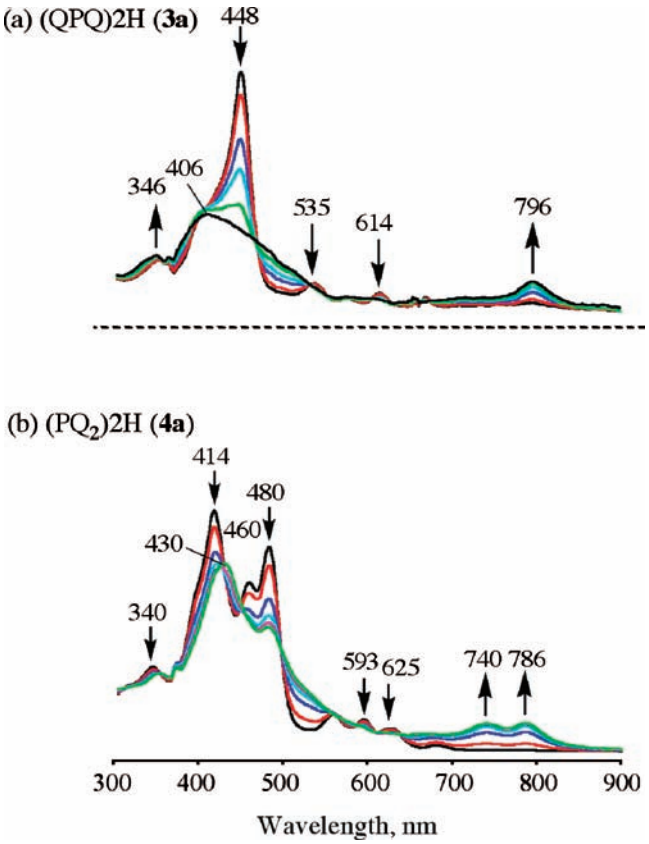

Figure 6. UV−vis spectral changes obtained during the first reduction of (a) (QPQ)2H (**3a**) and (b) (PQ_2)2H (**4a**) in CH_2Cl_2 containing 0.1 M TBAP. Applied potential: E_{app} = −1.25 and −1.40 V (vs SCE) for **3a** and **4a**, respectively.

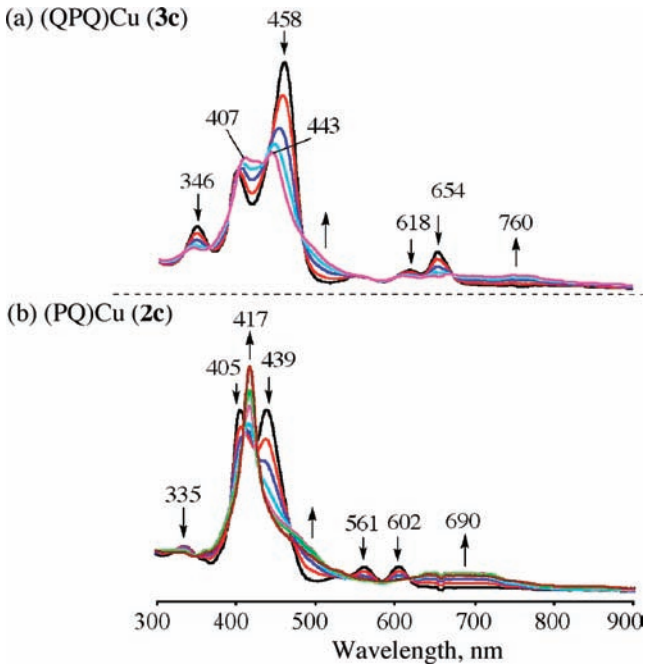

Figure 7. UV−vis spectral changes obtained during the first reduction of (a) (QPQ)Cu (**3c**) and (b) (PQ)Cu (**2c**) in CH_2Cl_2 containing 0.1 M TBAP. Applied potential: E_{app} = −1.15 and −1.40 V (vs SCE) for **3c** and **2c**, respectively.

is significantly red-shifted as compared with that of the radical anion for the monoquinoxalinoporphyrin (PQ)Cu (**2c**) (690 nm). This indicates more delocalized spin over the porphyrin and two quinoxaline units in the (QPQ)Cu (**3c**) radical anion as compared with the (PQ)Cu (**2c**) radical anion.[41]

In contrast to the spectral features of the radical anions, the radical cations of the bisqunoxalinoporphyrins exhibit broad absorption bands with absorption maxima similar to those of the monoquinoxalinoporphyrins. The spectra of these porphyrin π-radical cations are similar to each other, irrespective of the central metal ion. Typical examples of the spectral changes that occur during oxidation are shown in Figure 8 for (PQ_2)Cu (**4c**) and (PQ)Cu (**2c**).[42] The spectral data indicates that the HOMO orbital is mainly localized on the porphyrin macrocycle without delocalization onto the quinoxaline unit (vide supra).

Electronic Communication between the Two Quinoxaline Units. To determine whether the two quinoxaline moieties (Q) can communicate with each other through the central porphyrin in the radical anion forms of (PQ_2)M and (QPQ)M, electron spin resonance (ESR) spectra were measured for the radical anions of the 2H and Zn derivatives.[31,32] The radical anions of (PQ)M (**2**), (QPQ)M (**3**), and (PQ_2)M (**4**) (M = 2H and Zn) were produced by photoinduced electron transfer from dimeric 1-benzyl-1,4-dihydronicotinamide ($(BNA)_2$)[43] to the quinoxalinoporphyrins in MeCN as shown in Scheme 2. $(BNA)_2$ acts as a unique two-electron donor to produce 2 equiv of the radical anions of electron acceptors, because $BNA^{\bullet}$ formed upon dissociative electron-transfer oxidation of $(BNA)_2$ can transfer an additional electron to electron acceptors.[44]

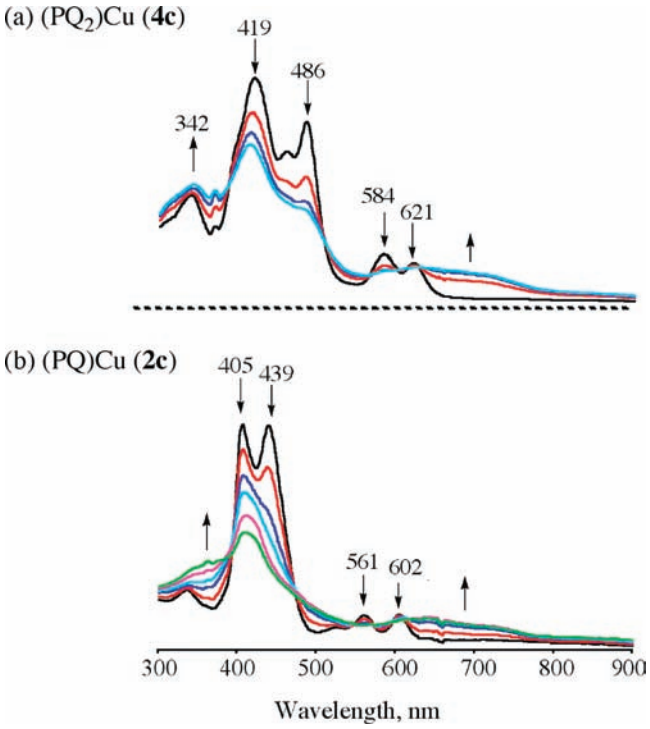

Figure 8. UV−vis spectral changes obtained during the first oxidation of (a) $(PQ_2)Cu$ (**4c**) and (b) (PQ)Cu (**2c**) in CH_2Cl_2 containing 0.1 M TBAP. Applied potential: E_{app} = 1.00 and 1.10 V (vs SCE) for **4c** and **2c**, respectively.

TABLE 2: DFT-Calculated Total and Nitrogen-Atom Spin-Density Ratios $P/Q_1/Q_2$ and P/Q/Q, in Comparison with ESR-Observed Nitrogen-Atom Hyperfine Coupling Constant Ratios for Atoms in the Porphyrin Macrocycle (P) and the Quinoxaline Groups (Q) of the Radical Anions

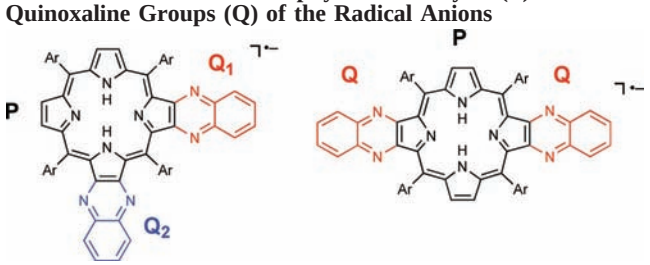

	nitrogen-atom contributions		total
molecule	ESR observed	DFT calculated	DFT calculated
(PQ)2H **2a**	69:31	80:20	90:10
$(PQ_2)2H^a$ (**4a**)	49:0:51	51:5:44	72:5:24
$(QPQ)2H^a$ (**3a**)	80:10:10	82:9:9	88:6:6
(PQ)Zn (**2b**)	66:34	62:38	76:24
$(PQ_2)Zn$ (**4b**)	48:34:18	48:30:22	73:14:13
(QPQ)Zn (**3b**)	47:27:27	66:17:17	74:13:13

[a] Structures for the corner (PQ_2) and linear (QPQ) species are shown above the table.

The hyperfine splitting of the observed radical anions combined with density functional theory (DFT) simulation of the calculated spin-density distribution provides valuable information on the degree of communication between two quinoxaline units, and the results obtained are summarized in Table 2. This table shows the observed ratio of total nitrogen-atom hyperfine coupling constants partitioned into contributions from each quinoxaline ring and the porphyrin ring, the corresponding ratio of calculated nitrogen-atom spin densities, and the total DFT-calculated spin density for each of the fragments. The observed nitrogen-atom hyperfine coupling constant ratios for atoms in the porphyrin macrocycle (P) and the quinoxaline groups (Q) of the bisquinoxalinoporphyrin radical anions largely agree with the ratios of the DFT-calculated spin densities as shown in Table 2.[45]

The ESR spectrum of radical anions of (PQ)2H (**2a**) obtained under photoirradiation of **2a** with $(BNA)_2$ is shown in Figure 9a. Hyperfine coupling constants of $[(PQ)2H]^{\bullet-}$ determined from this spectrum by computer simulation (see Experimental Section) (Figure 9b) indicate that the unpaired electron is delocalized on both the porphyrin and the quinoxaline units with a P/Q nitrogen-atom ratio of 69:31. This is similar to the nitrogen-atom spin-density ratio of 80:20 predicted by the DFT calculation (Figure 9c). However, as the calculations predict that the porphyrin carbon atoms take a disproportionate fraction of the unpaired electron, the calculated total spin-density ratio of 90:10 (Table 2) indicates that the radical is porphyrin-dominated. The DFT calculations also predict that the splitting between the porphyrin-based and the quinoxaline-based orbitals over which the charge is delocalized is 0.57 eV, the electronic coupling that drives delocalization is on the order of 10% × 0.57 = 0.06 eV. Such coupling would be sufficient to facilitate electron transport through one of these units if it were incorporated into a single-molecule conduction device. It should also be noted that no hyperfine splitting is observed for the free-base protons. This indicates that the tautomer of $[(PQ)2H]^{\bullet-}$ is locked in a position where the protons are attached to pyrroles that are not fused to the quinoxaline ring as is the case for neutral (PQ)2H (**2a**) (vide supra).

Similarly the ESR spectrum of the symmetric linear molecule $[(QPQ)2H]^{\bullet-}$, shown in Figure 10a together with its computer simulation spectrum (Figure 10b) and calculated spin distributions (Figure 10c), indicates that coupling occurs between the porphyrin and the quinoxaline units. This radical anion has D_{2h} symmetry when *a*N values for N(21) and N(23) should be the same. In such a case, however, the center line of the ESR signals would be the strongest to afford odd number lines. The apparent even number ESR lines observed in Figure 10a can only be reproduced by introducing inequivalent *a*N values for N(21) and N(23) as shown in Figure 10b. Such a break of the D_{2h} symmetry may be caused by the ion pair formation with the counter cation (BNA^+).[45] The extent of spin delocalization in the molecule $[(QPQ)2H]^{\bullet-}$, $P/Q_1/Q_2$ = 88:6:6, appears less than that seen for $[(PQ)2H]^{\bullet-}$. This again reflects a significant interaction as the DFT-calculated separation between the interacting orbitals is 0.58 eV.

The ESR spectrum of the asymmetric corner molecule $[(PQ_2)2H]^{\bullet-}$ obtained under photoirradiation of **4a** with $(BNA)_2$ (Figure 11a) looks very different from either that of $[(PQ)2H]^{\bullet-}$ or its linear isomer, $[(QPQ)2H]^{\bullet-}$. The total spin-density ratio, calculated to be $P/Q_1/Q_2$ = 72:5:24 (Table 2 and Figures 11b and 11c), indicates that the porphyrin interacts more strongly with one of the quinoxaline groups than the other.

ESR results showed that the porphyrin inner-ring hydrogen tautomer is observed to be locked, as indicated by the hyperfine interactions arising from just one pyrrole proton, confirming ^1H NMR spectral analysis. It is this symmetry-breaking effect that distinguishes the corner isomer from its linear counterpart: The pyrrole with an attached proton is more susceptible to reduction, bringing its energy into resonance with a porphyrin orbital. This effect is manifested by the large positive shift (160 mV) in the one-electron reduction potential of $(PQ_2)2H$ as compared with that of (PQ)2H (Figure 4).

In contrast to what is observed for the free-base bisquinoxalinoporphyrins (**4a** and **3a**), the ESR spectra of the radical

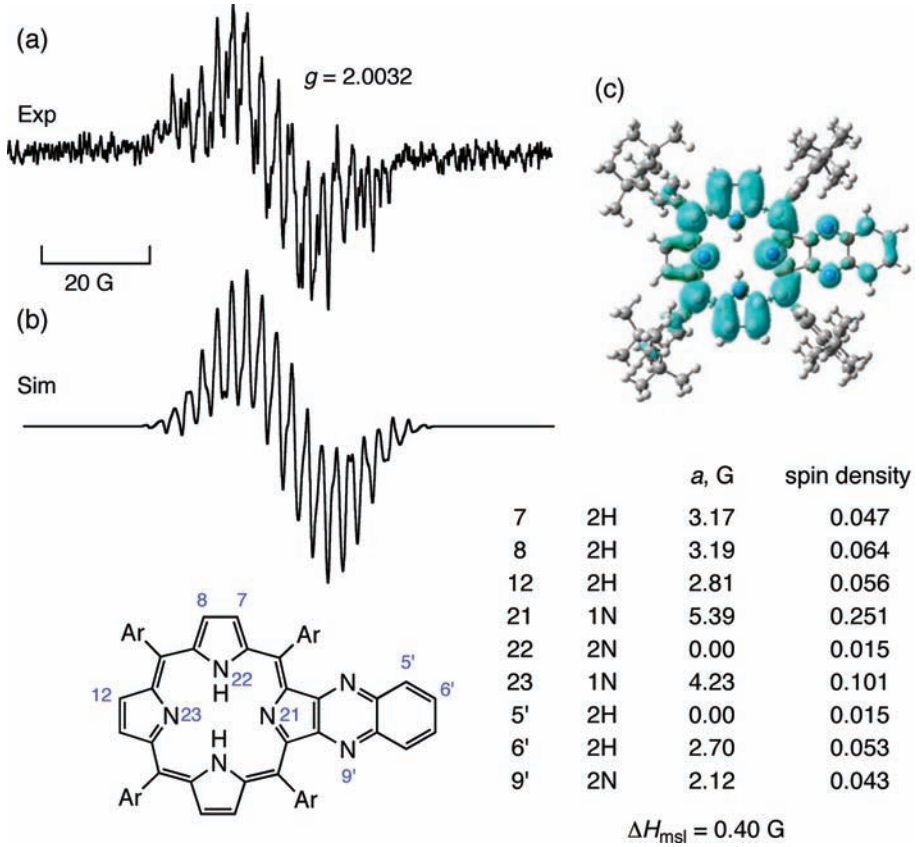

		a, G	spin density
7	2H	3.17	0.047
8	2H	3.19	0.064
12	2H	2.81	0.056
21	1N	5.39	0.251
22	2N	0.00	0.015
23	1N	4.23	0.101
5'	2H	0.00	0.015
6'	2H	2.70	0.053
9'	2N	2.12	0.043

ΔH_{msl} = 0.40 G

Figure 9. (a) ESR spectra of radical anions of (PQ)2H (**2a**) obtained under photoirradiation of **2a** with $(BNA)_2$. (b) Computer simulation spectrum with (c) hyperfine coupling constants and the distribution of spin densities calculated using DFT.

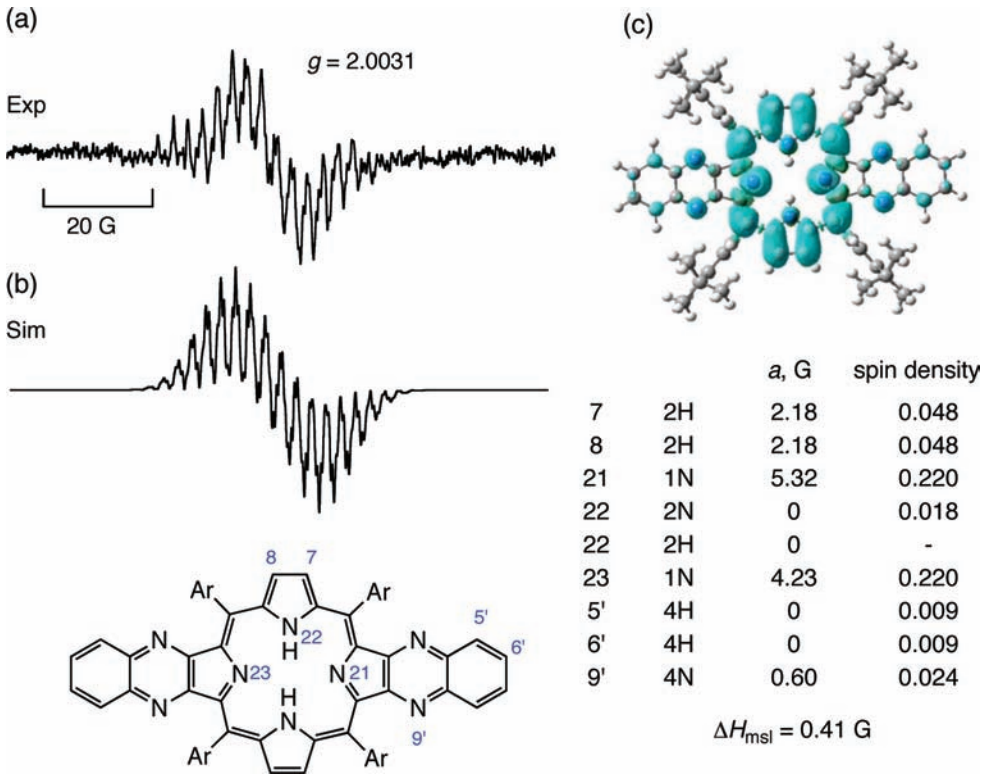

		a, G	spin density
7	2H	2.18	0.048
8	2H	2.18	0.048
21	1N	5.32	0.220
22	2N	0	0.018
22	2H	0	-
23	1N	4.23	0.220
5'	4H	0	0.009
6'	4H	0	0.009
9'	4N	0.60	0.024

ΔH_{msl} = 0.41 G

Figure 10. (a) ESR spectrum of the radical anion of (QPQ)2H (**3a**) obtained under photoirradiation of **3a** with $(BNA)_2$. (b) Computer simulation spectrum with (c) hyperfine coupling constants and the distribution of spin densities calculated using DFT.

anions of both zinc bisquinoxalinoporphyrins (**4b** and **3b**) together with the computer-simulated spectra[45] and the DFT-calculated spin densities indicate that there is significant communication between the two quinoxaline units on the molecule as shown in Figures 12 and 13. The enhanced coupling for the linear molecule (QPQ)Zn (**3b**), which increases the delocalization from $P/Q_1/Q_2 = 88:6:6$ for (QPQ)2H (**3a**) to 74:13:13, arises as zinc metalation destabilizes the porphyrin

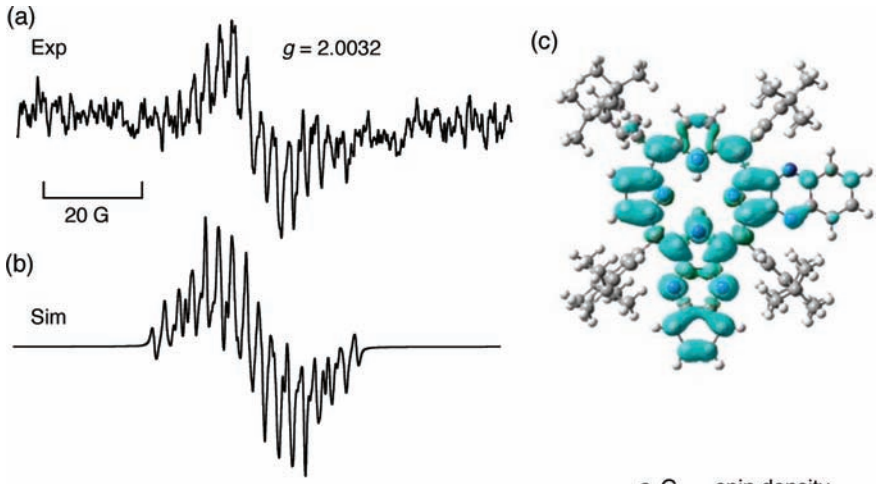

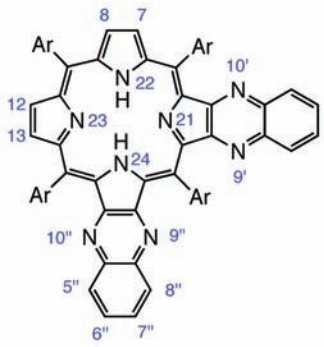

		a, G	spin density
7	1H	0	0.002
8	1H	0	0.000
12	1H	2.39	0.048
13	1H	0.30	0.027
21	1N	0	0.028
22	1N	2.48	0.051
22	1H	3.02	-
23	1N	0	0.026
24	1N	5.34	0.147
24	1H	4.10	-
9'	1N	0	0.017
10'	1N	0	0.006
5"	1H	0.30	0.026
6"	1H	0.30	0.031
7"	1H	0	0.014
8"	1H	0	0.021
9"	1N	4.10	0.114
10"	1N	4.10	0.105

ΔH_{msl} = 0.46 G

Figure 11. (a) ESR spectrum of the radical anion of $(PQ_2)2H$ **4a** obtained under photoirradiation of **4a** with $(BNA)_2$. (b) Computer simulation spectrum with (c) hyperfine coupling constants and the distribution of spin densities calculated using DFT.

SCHEME 2

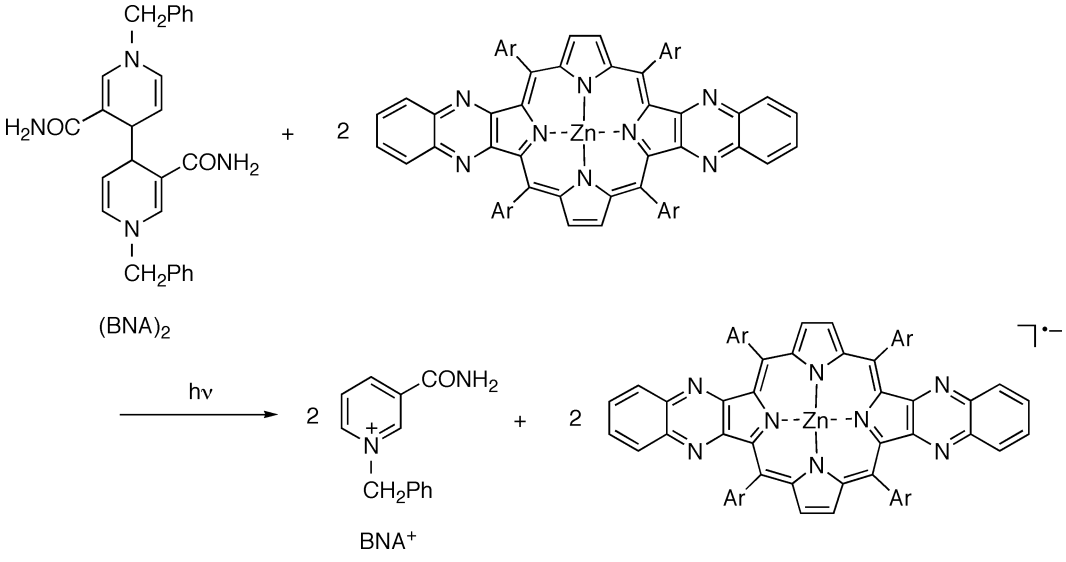

LUMO orbital, bringing it more into resonance with the quinoxaline orbitals. This effect is also observed for the monoquinoxalinoporphyrins (PQ)2H and (PQ)Zn. More profoundly, however, metalation of the corner molecule removes the inner NH protons that break the symmetry in the free-base analogue so that (PQ_2)Zn (**4b**) and (QPQ)Zn (**3b**) have very

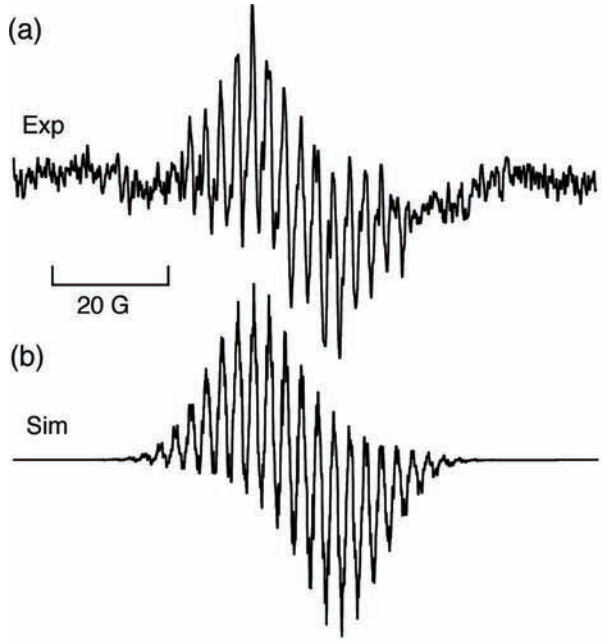

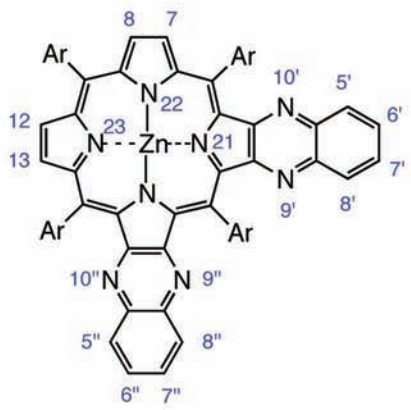

(c)

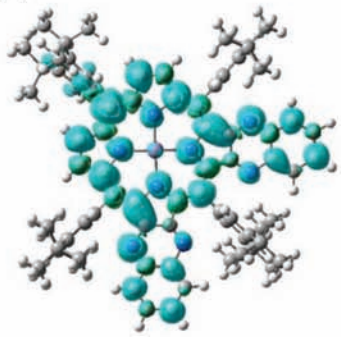

		a, G	spin density
7	1H	2.25	0.030
8	1H	3.26	0.066
12	1H	3.26	0.066
13	1H	1.98	0.030
21	1N	2.86	0.073
22	1N	2.65	0.035
23	1N	2.66	0.045
24	1N	2.86	0.051
5'	1H	2.66	0.038
6'	1H	0	0.013
7'	1H	2.66	0.037
8'	1H	0	0.003
9'	1N	2.66	0.021
10'	1N	5.28	0.105
5"	1H	2.25	0.033
6"	1H	0	0.001
7"	1H	1.98	0.021
8"	1H	0	0.006
9"	1N	0	0.008
10"	1N	4.24	0.089

ΔH_{msl} = 0.20 G

Figure 12. (a) ESR spectrum of the radical anion of (a) $(PQ_2)Zn$ (**4b**) obtained under photoirradiation of **4b** with $(BNA)_2$. (b) Computer simulation spectrum with (c) hyperfine coupling constants and the distribution of spin densities calculated using DFT.

similar spin densities. Hence, metalation eliminates the quinoxaline-orbital differentiation found for the free-base analogue of the corner molecule.

Corner Bisquinoxalinoporphyrins as Potential Molecular Rectifiers. Table 2 and Figures 11 and 12 indicate that the properties of the LUMO of the free-base and zinc(II) corner bisquinoxalinoporphyrins, $(PQ_2)2H$ (**4a**) and $(PQ_2)Zn$ (**4b**), are quite distinct. This will result in different electrical behavior when either compound is used in through-molecule electron transport by attaching the peripheral quinoxaline groups to external molecular wires or metallic leads. However, such conductivity arises not just from single orbitals, and therefore, an understanding of the properties of the nearby orbitals is also required. Shown in Figure 14 are the four lowest-energy unoccupied orbitals evaluated for the neutral zinc and free-base corner bisquinoxalinoporphyrins, along with their energies and the associated percentage localizations on the porphyrin and quinoxaline fragments. These percentages for the LUMOs differ slightly from those in Table 2 as this table shows spin densities evaluated for the radical anion species. A four-orbital model has been fitted to reproduce the orbital energies and percentages, considering one orbital included for each quinoxaline as well as two porphyrin orbitals. The resulting pure-component orbitals and their interaction energies are shown in Figure 15. All quinoxaline−porphyrin interaction strengths are significant, ranging from 0.16 to 0.26 eV. For $(PQ_2)Zn$ (**4b**), the orbital diagram corresponds to that for a tunneling barrier, allowing current to pass bidirectionally. For $(PQ_2)2H$ (**4a**), the orbital diagram corresponds to an Aviram−Ratner rectifier;[46] as when the potentials of the contact leads match the energy levels of the quinoxalines to which they are connected, current will flow; however, a large tunneling barrier is presented to current flow at reverse bias.

It can be seen that for through-porphyrin conduction using the Aviran−Ratner mechanism electrons must be injected

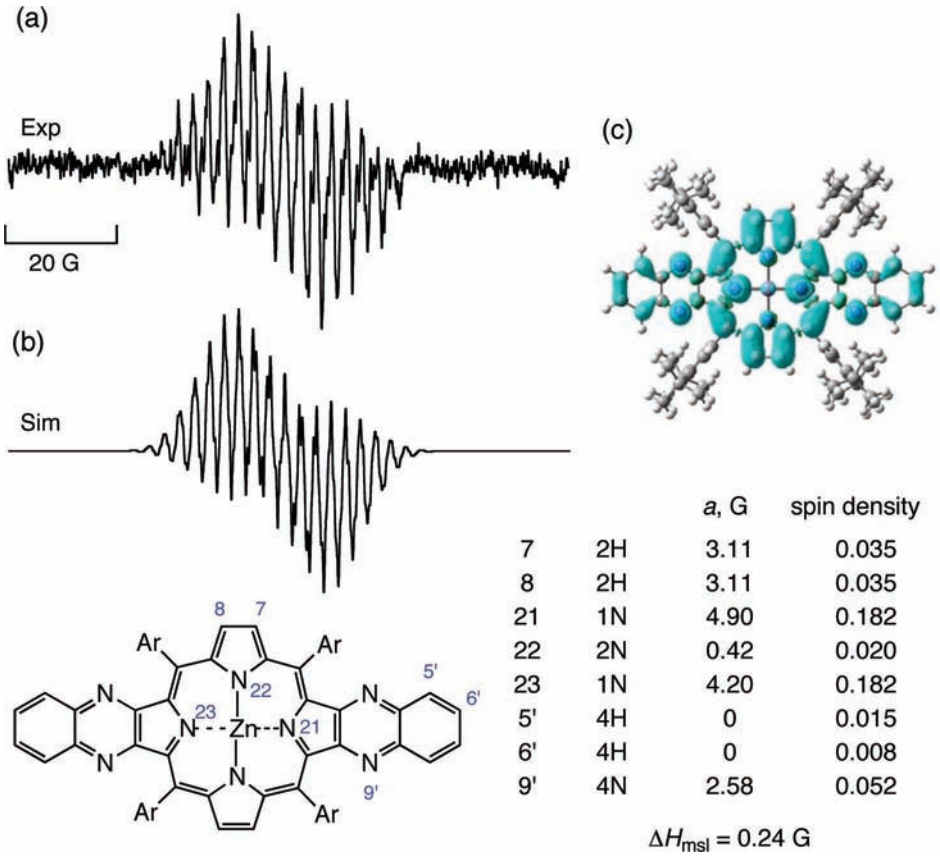

		a, G	spin density
7	2H	3.11	0.035
8	2H	3.11	0.035
21	1N	4.90	0.182
22	2N	0.42	0.020
23	1N	4.20	0.182
5'	4H	0	0.015
6'	4H	0	0.008
9'	4N	2.58	0.052

ΔH_{msl} = 0.24 G

Figure 13. (a) ESR spectrum of the radical anion of (QPQ)Zn (**3b**) obtained under photoirradiation of **3b** with $(BNA)_2$. (b) Computer simulation spectrum with (c) hyperfine coupling constants and the distribution of spin densities calculated using DFT.

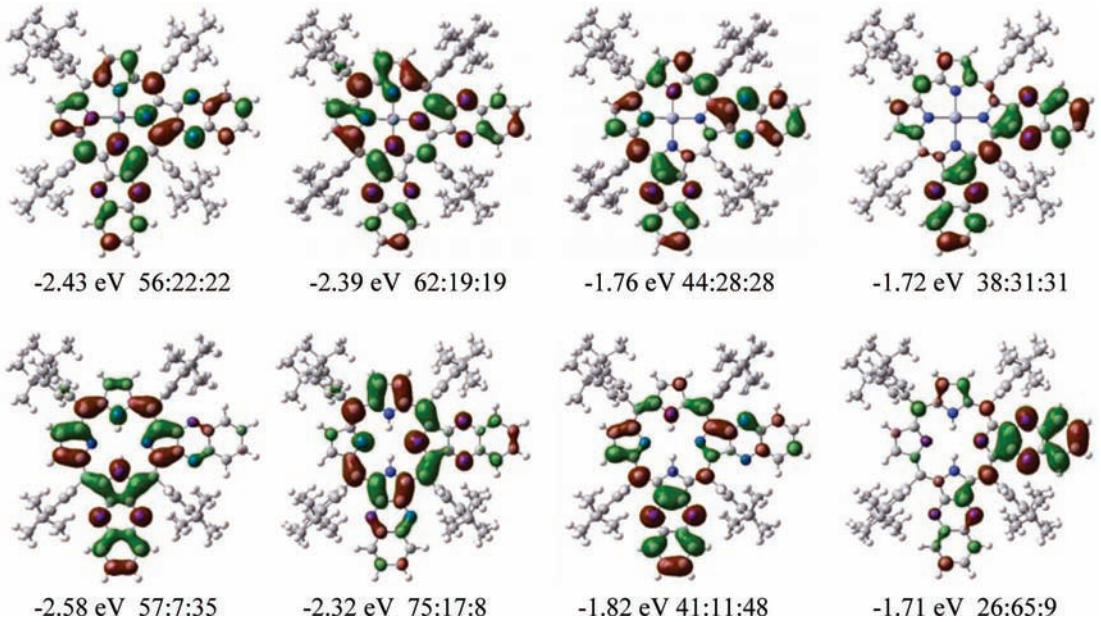

Figure 14. Four lowest-energy unoccupied orbitals for $(PQ_2)Zn$ (**4b**, top) and $(PQ_2)2H$ (**4a**, bottom) showing the orbital energy and the percentage of each orbital on the fragments $P/Q_1/Q_2$.

through the extended π-system attached to the pyrrolic group that is not protonated on the inner periphery of the macrocycle and leave via the extended π-system attached to the protonated pyrrolic group. To use this motif in a molecular device, it will be necessary to control the position of the inner hydrogens, along the *x*-axis or along the *y*-axis, depending on which direction it is desired for the flow of electrons, prior to reduction of the rectifying unit. It is envisaged that this can be accomplished by "locking" tautomerism through asymmetric substitution of the non-annulated pyrrolic rings of the porphyrin. This type of bias has been shown in simple tetraphenylporphyrins in earlier studies.[34] Regioselective incorporation of the rectifying unit into a "molecular wire" with an inbuilt redox gradient that will also contain external attachment sites should be straightforward using

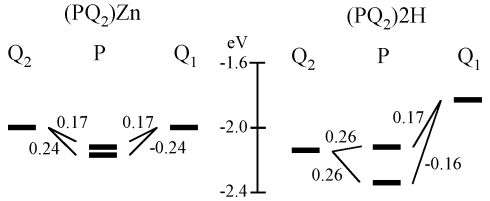

Figure 15. Isolated-component orbital energies and couplings (in eV) for corner bisquinoxalinoporphyrins (PQ_2)Zn (**4b**) and (PQ_2)2H (**4a**) fitted to reproduce the DFT-calculated orbital energies are percentage localizations shown in Figure 14.

methodologies developed for the construction of charge-shift compounds that model the PRC.[12,47,48]

Conclusions

This study indicates that the (QPQ)Zn (**3b**) macrocycle can be used to facilitate electron transport through a molecular wire with significant interaction of up to 0.25 eV between the porphyrin and the quinoxaline LUMOs. Also, the (PQ_2)Zn (**4b**) macrocycle can be used to facilitate a 90° bend in a molecular wire, having very similar electron-conductivity properties to that of its linear counterpart. Electrochemical analysis indicates that the Cu(II), Ni(II), and Pd(II) derivatives may act similarly. For the free-base analogues, however, the electrical properties of the unit are significantly altered. For the linear macrocycle, the primary effect is to slightly reduce the coupling, but the breaking of the molecular symmetry forced by the internal proton arrangement leads to (PQ_2)2H (**4a**) having the ability to act as a potential Aviram−Ratner rectifier,[46] passing electrons only when they enter from the direction of the non-protonated pyrrolic ring. Although any rectifier requires electrical contacts in the solid state, the degree of electron spin delocalization into the fused rings in the π-radical anions of the free-base and metal(II) bisquinoxalinoporphyrins elucidated in this study provides valuable chemical basis for design of the architecture of a chemically controlled rectifier.

Experimental Section

General Procedure. Melting points were recorded on a Reichert melting point stage and are uncorrected. Microanalyses were performed by the Campbell Microanalytical Laboratory, University of Otago, New Zealand. Infrared spectra were recorded on Perkin-Elmer model 1600 and FTIR-8400S SHIMADZU Fourier transform infrared spectrophotometers, as solutions in the stated solvents. Intensity abbreviations used are: w, weak; m, medium; s, strong; br, broad. UV−vis spectra were routinely recorded on a Cary 5E UV−vis−near-IR spectrophotometer in chloroform that was deacidified by filtration through an alumina column. ^{1}H NMR spectra were recorded on a Bruker DPX-400 (400 MHz) spectrometer. Samples were dissolved in $CDCl_3$, and the chloroform peak at 7.26 was used as an internal reference unless otherwise stated. Deuterated solvents were used as received except for deuterated chloroform, which was deacidified by filtration through a plug of alumina. Signals were recorded in terms of chemical shifts (in ppm), relative integral, multiplicity, coupling constants (in Hz), and assignment, in that order. The following abbreviations for multiplicity are used: s, singlet; d, doublet; dd, doublet of doublets; t, triplet; m, multiplet; br, broad; ABq, AB quartet; d of ABq, doublet of AB quartet.

Matrix-assisted laser desorption ionization time-of-flight (MALDI-TOF) mass spectra were recorded on a VG TofSpec spectrometer. Electrospray ionization (ESI) and atmospheric pressure chemical ionization (APCI) mass spectra were recorded on a ThermoQuest Finnigan LCQ DECA instrument. High-resolution electrospray ionization Fourier transform ion cyclotron resonance (HR-ESI-FT/ICR) spectra were acquired at the Research School of Chemistry, The University of New South Wales, on a Bruker Daltonics BioAPEX II FT/ICR mass spectrometer equipped with a 4.7 T MAGNEX superconducting magnet and an Analytica external ESI source. Electrospray ionization high-resolution mass spectrometry (ESI-HRMS) was performed on a VG Quattro II triple quadrupole mass spectrometer at the Research School of Chemistry, Australian National University.

Column chromatography was routinely carried out using the gravity feed column technique on Merck silica gel type 9385 (230−400 mesh). Analytical thin-layer chromatography (TLC) analyses were performed on Merck silica gel 60 F_{254} precoated sheets (0.2 mm). Alumina refers to Merck aluminum oxide 90 active neutral I, type 1077. All commercial solvents were routinely distilled prior to use. Light petroleum refers to the fraction of bp 60−80 °C. Ethanol-free chloroform was obtained by drying distilled chloroform over calcium chloride and passing through a column of alumina immediately prior to use. Where solvent mixtures were used, the proportions are given by volume. Analytically pure samples of **3a**−**e** and **4a**−**e** were obtained by recrystallization from a chloroform−methanol solution.

5,10,15,20-Tetrakis(3,5-di-*tert*-butylphenyl)bisquinoxalino[2,3-*b*′:12,13-*b*″]porphyrin (3a). 2,3,12,13-Tetraoxo-5,10,15,20-tetrakis(3,5-di-*tert*-butylphenyl)bacteriochlorin (**5**)[27] (130 mg, 0.116 mmol) and *o*-phenylenediamine (**6**) (85.0 mg, 0.786 mmol) were dissolved in dichloromethane (20 mL) and stirred at room temperature for 10 min. The solvent was removed under vacuum, and the crude residue was purified by chromatography over silica (chloroform−light petroleum; 1:3). The major front running brown band was collected and evaporated to afford 5,10,15,20-tetrakis(3,5-di-*tert*-butylphenyl)bisquinoxalino[2,3-*b*′:12,13-*b*″]porphyrin (**3a**) (106 mg, 72%) as a purple microcrystalline solid, mp >300 °C. IR ($CHCl_3$): 3383w, 3058w, 3028w, 3019s, 2964s, 2903m, 2867m, 1594s, 1495w, 1477m, 1428w, 1393w, 1363m, 1347w, 1299m, 1248m, 1223m, 1207m, 1199w, 1154m, 1132w, 1108s, 1009w, 946w, 926w, 901m cm^{-1}. UV−vis ($CHCl_3$): 351 (log ϵ 4.57), 398sh (4.90), 449 (5.41), 495sh (3.82), 533 (4.38), 570sh (3.75), 614 (4.14), 668 (4.12) nm. ^{1}H NMR (400 MHz, $CDCl_3$) δ: −2.48 (2 H, s, inner NH); 1.49 (72 H, s, *t*-butyl H); 7.73−7.77 (4 H, m, quinoxaline H); 7.82−7.87 (4 H, m, quinoxaline H); 7.94 (4 H, t, *J* 1.8 Hz, Hp); 7.99 (8 H, d, *J* 1.8 Hz, Ho); 9.09 (4 H, d, *J* 1.8 Hz, β-pyrrolic H). MS (ESI) (*m*/*z*): 1267.9 (M^+ requires 1267.8). Anal. calcd. for $C_{88}H_{98}N_8$: C, 83.37; H, 7.79; N, 8.84. Found: C, 83.26; H, 7.89; N, 8.62.

{5,10,15,20-Tetrakis(3,5-di-*tert*-butylphenyl)bisquinoxalino[2,3-*b*′:12,13-*b*″]porphyrinato}zinc(II) (3b). 5,10,15,20-Tetrakis(3,5-di-*tert*-butylphenyl)bisquinoxalino[2,3-*b*′:12,13-*b*″]-porphyrin (**3a**) (59.0 mg, 0.0465 mmol) and zinc(II) acetate dihydrate (70.0 mg, 0.319 mmol) were dissolved in a solution of chloroform (40 mL) and methanol (20 mL). The mixture was then heated at reflux for 18 h. The solvent was removed under vacuum, and the residue was purified by column chromatography over silica (dichloromethane−light petroleum; 1:1). The front running green band was collected, and the solvent was removed to afford {5,10,15,20-tetrakis(3,5-di-*tert*-butylphenyl)bisquinoxalino[2,3-*b*′:12,13-*b*″]porphyrinato}zinc(II) (**3b**) (56.0 mg, 90%) as a green microcrystalline solid, mp >300 °C. IR ($CHCl_3$): 3057w, 2020m, 3016m, 2964s, 2903m,

2866m, 1593s, 1477m, 1464w, 1429w, 1393w, 1362m, 1340w, 1312w, 1300w, 1248w, 1215s, 1204s, 1169m, 1113w, 1036w, 949m cm^{-1}. UV−vis ($CHCl_3$): 345 (log ϵ 4.63), 405 (5.04), 465 (5.25), 556 (4.01), 582 (3.83), 601 (4.07), 637 (4.18), 655 (4.71) nm. ^1H NMR (400 MHz, $CDCl_3$) δ: 1.50 (72 H, s, *t*-butyl H); 7.78−7.82 (4 H, m, quinoxaline H); 7.90−7.93 (4 H, m, quinoxaline H); 7.95 (4 H, t, *J* 1.8 Hz, Hp); 7.99 (8 H, d, *J* 1.8 Hz, Ho); 9.14 (4 H, s, β-pyrrolic H). MS (ESI) (*m*/*z*): 1332.0 (M^+ requires 1331.2). MS (MALDI-TOF) (*m*/*z*): 1332 (M^+ requires 1331). (ESI-HRMS $C_{88}H_{96}N_8Zn$ requires 1329.712. Found: $[M + H]^+$ 1329.716.). Anal. calcd. for $C_{88}H_{96}N_8Zn + 2CH_3OH$: C, 77.48; H, 7.51; N, 8.05. Found: C, 77.42; H, 7.22; N, 8.25.

{5,10,15,20-Tetrakis(3,5-di-*tert*-butylphenyl)bisquinoxalino-[2,3-*b*′:12,13-*b*″]porphyrinato}copper(II) (3c). 5,10,15,20-Tetrakis(3,5-di-*tert*-butylphenyl)bisquinoxalino[2,3-*b*′:12,13-*b*″]porphyrin (**3a**) (105 mg, 0.0830 mmol) and copper(II) acetate monohydrate (214 mg, 1.07 mmol) were dissolved in a solution of chloroform (80 mL) and methanol (40 mL). The mixture was heated at reflux for 4 h. The solvent was removed under vacuum, and the residue was washed through a plug of silica (dichloromethane−light petroleum; 1:2). The major green band was collected, and the solvent was removed to afford {5,10,-15,20-tetrakis(3,5-di-*tert*-butylphenyl)-bisquinoxalino[2,3-*b*′:12,-13-*b*″]porphyrinato}copper(II) (**3c**) (100 mg, 91%) as a dark green microcrystalline solid, mp >300 °C. IR ($CHCl_3$): 3054w, 3025s, 2991w, 2962s, 1595s, 1493w, 1477m, 1426w, 1394w, 1363s, 1299m, 1248w, 1236w, 1226s, 1200w, 1176m, 1117m, 1008m, 950m, 900w cm^{-1}. UV−vis ($CHCl_3$): 346 (log ϵ 4.73), 398 (5.01), 459 (5.27), 548 (4.02), 567sh (3.94), 608sh (4.08), 618 (4.14), 655 (4.49) nm. MS (ESI) (*m*/*z*): 1329.7 (M^+ requires 1329.3). MS (MALDI-TOF) (*m*/*z*): 1330 (M^+ requires 1329). Anal. calcd. for $C_{88}H_{96}N_8Cu$: C, 79.50; H, 7.28; N, 8.43. Found: C, 79.90; H, 7.20; N, 8.08.

{5,10,15,20-Tetrakis(3,5-di-*tert*-butylphenyl)bisquinoxalino-[2,3-*b*′:12,13-*b*″]porphyrinato}nickel(II) (3d). 5,10,15,20-Tetrakis(3,5-di-*tert*-butylphenyl)bisquinoxalino[2,3-*b*′:12,13-*b*″]-porphyrin (**3a**) (42.0 mg, 0.0331 mmol) and nickel(II) acetate dihydrate (56.0 mg, 0.263 mmol) were dissolved in dissolved in a solution of toluene (7 mL) and glacial acetic acid (18 M, 7 mL). The mixture was then heated at reflux for 18 h. Dichloromethane (30 mL) was added to the mixture, and the organic phase was separated, washed with water (200 mL), sodium carbonate solution (10%, 2 × 150 mL), and water (200 mL), dried over anhydrous sodium sulfate, filtered, and evaporated to dryness. The residue was purified by column chromatography over silica (chloroform−light petroleum; 1:2), the front running green band was collected, and the solvent was removed to afford 5,10,15,20-tetrakis(3,5-di-*tert*-butylphenyl)bisquinoxalino[2,3-*b*′:12,13-*b*″]porphyrinato}nickel(II) (**3d**) (39.3 mg, 90%) as a green microcrystalline solid, mp >300 °C. IR ($CHCl_3$): 2967s, 2906m, 2868m, 1595s, 1478m, 1393w, 1364s, 1249m, 1179m, 1041w cm^{-1}. UV−vis ($CHCl_3$): 361 (log ϵ 4.83), 404 (4.80), 465 (5.14), 551 (3.94), 618 (4.03), 662 (4.35) nm. ^1H NMR (400 MHz, $CDCl_3$) δ: 1.46 (72 H, s, *t*-butyl H); 7.76 (8 H, d, *J* 1.6 Hz, Ho); 7.77−7.79 (4 H, m, quinoxaline H); 7.83−7.86 (8 H, m, quinoxaline H, Hp); 9.01 (4 H, s, β-pyrrolic H). MS (ESI) (*m*/*z*): 1324.1 (M^+ requires 1324.5). Anal. calcd. for $C_{88}H_{96}N_8Ni$: C, 79.80; H, 7.31; N, 8.46. Found: C, 80.07; H, 7.26; N, 8.55.

{5,10,15,20-Tetrakis(3,5-di-*tert*-butylphenyl)bisquinoxalino-[2,3-*b*′:12,13-*b*″]porphyrinato}palladium(II) (3e). 5,10,15,-20-Tetrakis(3,5-di-*tert*-butylphenyl)bisquinoxalino[2,3-*b*′:12,13-*b*″]porphyrin (**3a**) (42.0 mg, 0.0331 mmol), palladium(II) chloride (37.0 mg, 0.209 mmol), and sodium acetate (33.0 mg, 0.402 mmol) were dissolved in a solution of toluene (10 mL) and glacial acetic acid (18 M, 10 mL). The mixture was then heated at reflux for 1 h. Dichloromethane (30 mL) was added to the mixture, and the organic phase was separated, washed with water (200 mL), sodium carbonate solution (10%, 2 × 150 mL), and water (200 mL), dried over anhydrous sodium sulfate, filtered, and evaporated to dryness. The residue was purified by column chromatography over silica (dichloromethane−light petroleum; 1:2), the front running green purple band was collected, and the solvent was evaporated to give 5,10,15,20-tetrakis(3,5-di-*tert*-butylphenyl)bisquinoxalino[2,3-*b*′:12,13-*b*″]-porphyrinato}palladium(II) (**3e**) (44.0 mg, 97%) as a purple needle solid, mp >300 °C. IR ($CHCl_3$): 3057w, 2964s, 2903m, 2868m, 1595s, 1495w, 1477m, 1460w, 1420w, 1393w, 1362s, 1327w, 1304w, 1248m, 1215m, 1204s, 1178m, 1134w, 1118w, 1045m, 957m cm^{-1}. UV−vis ($CHCl_3$): 351 (log ϵ 4.87), 395 (4.91), 452 (5.23), 531 (4.08), 546sh (3.92), 686 (4.13), 597sh (4.04), 631 (4.82) nm. ^1H NMR (400 MHz, $CDCl_3$) δ: 1.48 (72 H, s, *t*-butyl H); 7.77−7.81 (4 H, m, quinoxaline H); 7.84−7.86 (4 H, m, quinoxaline H); 7.92−7.93 (12 H, m, Ho, Hp); 8.97 (4 H, s, β-pyrrolic H). MS (ESI) (*m*/*z*): 1372.0 (M^+ requires 1372.2). (HR-ESI-FT/ICR Found: $[M + H]^+$ 1371.6928. $C_{88}H_{96}N_8Pd$ requires 1371.6895.) Anal. calcd. for $C_{88}H_{96}N_8Pd$: C, 77.03; H, 7.05; N, 8.17. Found: C, 76.55; H, 6.99; N, 8.06.

5,10,15,20-Tetrakis(3,5-di-*tert*-butylphenyl)bisquinoxalino-[2,3-*b*′:7,8-*b*″]porphyrin (4a). A mixture of 2,3,7,8-tetraoxo-5,10,15,20-tetrakis(3,5-di-*tert*-butylphenyl)isobacteriochlorin (**7**)[27] (54 mg, 0.0481 mmol) and *o*-phenylenediamine (**6**) (15.7 mg, 0.145 mmol) were dissolved in dichloromethane (10 mL) and stirred at room temperature for 10 min. The reaction mixture was evaporated to dryness, and the crude residue wsa purified by chromatography over silica (dichloromethane−light petroleum; 1:2). The front running brown band was collected, and the solvent was removed under vacuum to give 5,10,15,20-tetrakis(3,5-di-*tert*-butylphenyl)-bisquinoxalino[2,3-*b*′:7,8-*b*″]-porphyrin (**4a**) (56.0 mg, 94%) as a dark purple microcrystalline solid, mp >300 °C. IR ($CHCl_3$): 3312w, 3058w, 3025s, 3011w, 2964s, 2903m, 2866m, 1595s, 1551w, 1476m, 1426w, 1393w, 1363s, 1297m, 1248m, 1233m, 1226s, 1211s, 1194w, 1157w, 1112m, 1000w, 984w, 933w cm^{-1}. UV−vis ($CHCl_3$): 314sh (log ϵ 4.49), 341 (4.60), 395sh (4.91), 416 (5.07), 456 (4.94), 482 (5.04), 559 (4.27), 595 (4.20), 626 (4.05), 678 (3.43) nm. ^1H NMR (400 MHz, $CDCl_3$) δ: −0.55 (2 H, br, s, inner NH); 1.45 (18 H, s, *t*-butyl H); 1.49 (36 H, s, *t*-butyl H); 1.53 (18 H, s, *t*-butyl H); 7.79−7.82 (5 H, m, aryl H); 7.84−7.87 (2 H, m, quinoxaline H); 7.89−7.93 (10 H, m, quinoxaline H, Ho, Hp); 8.02 (1 H, t, *J* 1.7 Hz, Hp); 8.06 (2 H, d, *J* 1.9 Hz, Ho); 8.68 and 8.72 (4 H, ABq, *J* 4.7 Hz, β-pyrrolic H). MS (ESI) (*m*/*z*): 1267.9 (M^+ requires 1267.8). Anal. calcd. for $C_{88}H_{98}N_8$: C, 83.4; H, 7.8; N, 8.8. Found: C, 83.6; H, 8.1; N, 8.4.

{5,10,15,20-Tetrakis(3,5-di-*tert*-butylphenyl)bisquinoxalino-[2,3-*b*′:7,8-*b*″]porphyrinato}zinc(II) (4b). A solution of 5,-10,15,20-tetrakis(3,5-di-*tert*-butylphenyl)bisquinoxalino[2,3-*b*′:7,8-*b*″]porphyrin (**4a**) (40.6 mg, 0.0320 mmol) and zinc(II) acetate monohydrate (28.0 mg, 0.128 mmol) was dissolved in a solution of chloroform (30 mL) and methanol (15 mL), and the mixture was heated at reflux for 3 min. The solvent was removed under vacuum, and the residue was passed through a plug of silica (dichloromethane−light petroleum; 1:1). The front running green band was collected, and the solvent was removed to give pure {5,10,15,20-tetrakis(3,5-di-*tert*-butylphenyl)bisquinoxalino[2,3-*b*′:7,8-*b*″]porphyrinato}zinc(II) (**4b**) (42.0 mg,

99%) as a dark green microcrystalline solid, mp >300 °C. IR ($CHCl_3$): 3059w, 3023s, 3014m, 2964s, 2903m, 2867m, 1594s, 1516w, 1477m, 1427w, 1392m, 1362s, 1345m, 1298m, 1248m, 1234m, 1222m, 1212m, 1170m, 1117m, 1093w, 1070w, 1036w, 1004m, 951m, 924w cm^{-1}. UV−vis ($CHCl_3$): 340 (log ϵ 4.60), 405sh (4.94), 423 (5.04), 465 (4.84), 494 (4.95), 539sh (3.89), 586sh (4.30), 596 (4.41), 629 (3.99) nm. ^1H NMR (400 MHz, $CDCl_3$) δ: 1.48 (18 H, s, *t*-butyl H); 1.51 (36 H, s, *t*-butyl H); 1.53 (18 H, s, *t*-butyl H); 7.79−7.81 (5 H, m, quinoxaline H, Hp); 7.87−7.94 (12 H, m, quinoxaline H, Ho, Hp); 8.04 (1 H, t, *J* 1.6 Hz, Hp); 8.09 (2 H, d, *J* 1.6 Hz, Ho); 8.88 and 8.91 (4 H, ABq, *J* 4.5 Hz, β-pyrrolic H). MS (ESI) (*m*/*z*): 1331.8 (M^+ requires 1331.2). Anal. calcd. for $C_{88}H_{96}N_8Zn$: C, 79.4; H, 7.3; N, 8.4. Found: C, 79.1; H, 7.5; N, 8.0.

{5,10,15,20-Tetrakis(3,5-di-*tert*-butylphenyl)bisquinoxalino-[2,3-*b*′:7,8-*b*″]porphyrinato}copper(II) (4c). 5,10,15,20-Tetrakis(3,5-di-*tert*-butylphenyl)bisquinoxalino[2,3-*b*′:7,8-*b*″]porphyrin (**4a**) (470 mg, 0.371 mmol) and copper(II) acetate monohydrate (556 mg, 2.79 mmol) in a solution of chloroform (80 mL) and methanol (40 mL) were heated at reflux for 10 min. The solvent was removed under vacuum, and the residue was passed through a plug of silica (dichloromethane−light petroleum; 1:3). The front running green band was collected, and the solvent was removed to afford {5,10,15,20-tetrakis(3,5-di-*tert*-butylphenyl)bisquinoxalino[2,3-*b*′:7,8-*b*″]porphyrinato}-copper(II) (**4c**) (485 mg, 98%) as a dark green microcrystalline solid, mp >300 °C. IR ($CHCl_3$): 3069w, 3046w, 3020s, 2964s, 2904m, 2868m, 1595s, 1529w, 1492w, 1477m, 1427w, 1393w, 1363s, 1349m, 1296m, 1248m, 1228m, 1222s, 1176s, 1116w, 1072w, 1034w, 1008w cm^{-1}. UV−vis ($CHCl_3$): 328sh (log ϵ 4.56), 339 (4.61), 397sh (4.79), 419 (4.94), 429sh (4.91), 462 (4.78), 488 (4.88), 584 (4.28), 621 (4.21) nm. MS (ESI) (*m*/*z*): 1329.8 (M^+ requires 1329.3). MS (MALDI-TOF) (*m*/*z*): 1329 (M^+ requires 1329). Anal. calcd. for $C_{88}H_{96}N_8Cu$: C, 79.5; H, 7.3; N, 8.4. Found: C, 79.5; H, 7.4; N, 8.1.

{5,10,15,20-Tetrakis(3,5-di-*tert*-butylphenyl)bisquinoxalino-[2,3-*b*′:7,8-*b*″]porphyrinato}nickel(II) (4d). 5,10,15,20-Tetrakis(3,5-di-*tert*-butylphenyl)bisquinoxalino[2,3-*b*′:7,8-*b*″]porphyrin (**4a**) (44.0 mg, 0.0347 mmol) and nickel(II) acetate tetrahydrate (30.0 mg, 0.141 mmol) were dissolved in a solution of toluene (10 mL) and glacial acetic acid (10 mL), and the mixture was heated at reflux for 1 min. Dichloromethane (30 mL) was added to the mixture, and the organic phase was separated, washed with water (200 mL), sodium carbonate solution (10%, 2 × 200 mL), and water (200 mL), dried over anhydrous sodium sulfate, filtered, and evaporated to dryness. The crude mixture was purified by column chromatography over silica (dichloromethane−light petroleum; 1:3). The front running green band was collected, and the solvent was removed to give 5,10,15,20-tetrakis(3,5-di-*tert*-butylphenyl)bisquinoxalino[2,3-*b*′:7,8-*b*″]porphyrinato}nickel(II) (**4d**) (45.5 mg, 99%) as a green microcrystalline solid, mp >300 °C. IR ($CHCl_3$): 3059w, 3018s, 2964s, 2904m, 2867m, 1595s, 1477w, 1427w, 1392w, 1364m, 1298w, 1247m, 1224s, 1177w, 1119w, 1016w, 952w cm^{-1}. UV−vis ($CHCl_3$): 314sh (log ϵ 4.48), 340sh (4.68), 355 (4.69), 399sh (4.69), 421sh (4.79), 436 (4.82), 466 (4.72), 491 (4.81), 584 (4.18), 622 (4.20) nm. ^1H NMR (400 MHz, $CDCl_3$) δ: 1.40 (18 H, s, *t*-butyl H); 1.43 (36 H, s, *t*-butyl H); 1.46 (18 H, s, *t*-butyl H); 7.65 (2 H, d, *J* 1.7 Hz, Ho); 7.69−7.70 (5 H, m, Ho, Hp); 7.73−7.77 (4 H, m, quinoxaline H); 7.79−7.82 (4 H, m, Hp, quinoxaline H); 7.83 (1 H, d, *J* 1.7 Hz, Ho); 7.88 (1 H, t, *J* 1.7 Hz, Hp); 7.91−7.94 (2 H, m, quinoxaline H); 8.65 and 8.78 (4 H, ABq, *J* 4.9 Hz, β-pyrrolic H). MS (ESI) (*m*/*z*): 1324.8 (M^+ requires 1324.5). MS (MALDI-TOF) (*m*/*z*): 1325 (M^+ requires 1325). Anal. calcd. for $C_{88}H_{96}N_8Ni$: C, 79.8; H, 7.3; N, 8.5. Found: C, 79.8; H, 7.5; N, 8.1.

{5,10,15,20-Tetrakis(3,5-di-*tert*-butylphenyl)bisquinoxalino-[2,3-*b*′:7,8-*b*″]porphyrinato}palladium(II) (4e). 5,10,15,20-Tetrakis(3,5-di-*tert*-butylphenyl)bisquinoxalino[2,3-*b*′:7,8-*b*″]-porphyrin (**4a**) (80.0 mg, 0.0631 mmol), palladium(II) chloride (70.0 mg, 0.395 mmol), and sodium acetate (79.0 mg, 0.963 mmol) were dissolved in a solution of toluene (13 mL) and glacial acetic acid (18 M, 13 mL). The mixture was then heated at reflux for 5 min. Dichloromethane (30 mL) was added to the mixture, and the organic phase was separated, washed with water (200 mL), sodium carbonate solution (10%, 2 × 150 mL), and water (200 mL), dried over anhydrous sodium sulfate, filtered, and evaporated to dryness. The crude mixture was purified by column chromatography over silica (dichloromethane−light petroleum; 1:3). The front running red band was collected, and the solvent was removed to give 5,10,15,20-tetrakis(3,5-di-*tert*-butylphenyl)bisquinoxalino[2,3-b′:7,8-b″]porphyrinato}-palladium(II) (**4e**) (86.0 mg, 99%) as a red microcrystalline solid, mp >300 °C. IR ($CHCl_3$): 3022m, 3014m, 3007w, 2964s, 2903m, 2868m, 1595s, 1537w, 1495w, 1477m, 1462w, 1427w, 1393w, 1364s, 1300m, 1248m, 1234m, 1217s, 1203m, 1178w, 1121w, 1018m, 1005w cm^{-1}. UV−vis ($CHCl_3$): 332 (log ϵ 4.68), 347 (4.69), 390sh (4.77), 423 (4.94), 452 (4.87), 476 (4.93), 564 (4.39), 599 (4.54) nm. ^1H NMR (400 MHz, $CDCl_3$) δ: 1.44 (18 H, s, *t*-butyl H); 1.48 (36 H, s, *t*-butyl H); 1.52 (18 H, s, *t*-butyl H); 7.78−7.92 (17 H, m, quinoxaline H, Ho, Hp); 8.03 (1 H, t, *J* 1.5 Hz, Hp); 8.04 (2 H, d, *J* 1.6 Hz, Ho); 8.80 and 8.88 (4 H, ABq, *J* 4.9 Hz, β-pyrrolic H). MS (ESI) (*m*/*z*): 1372.7 (M^+ requires 1372.2). MS (MALDI-TOF) (*m*/*z*): 1373 (M^+ requires 1372). (HR-ESI-FT/ICR Found: $[M + H]^+$ 1371.6890. $C_{88}H_{96}N_8Pd$ requires 1371.6895.) Anal. calcd. for $C_{88}H_{96}N_8Pd + CH_3OH$: 76.13; H, 7.18; N, 7.98. Found: C, 76.09; H, 7.07; N, 8.07.

Electrochemical Measurements. Cyclic voltammetry was carried out by using an EG&G Princeton Applied Research (PAR) 173 potentiostat/galvanostat. A homemade three-electrode cell was used for cyclic voltammetric measurement and consisted of a platinum button or glassy carbon working electrode, a platinum counter electrode, and a homemade saturated calomel reference electrode (SCE). The SCE was separated from the bulk of the solution by a fritted glass bridge of low porosity which contained the solvent/supporting electrolyte mixture. UV−vis spectroelectrochemical experiments were performed with a home-built thin-layer cell that had a light transparent platinum net working electrode. Potentials were applied and monitored with an EG&G PAR model 173 potentiostat. Time-resolved UV−vis spectra were recorded with a Hewlett-Packard model 8453 diode array spectrophotometer. Absolute CH_2Cl_2 from Aldrich Co. was used as received without further purification. TBAP was purchased from Sigma Chemical or Fluka Chemika Co., recrystallized from ethyl alcohol, and dried under vacuum at 40 °C for at least 1 week prior to use.

ESR Measurements. Radical anions of the quinoxalinoporphyrins were prepared by the photoreduction of the compounds with $(BNA)_2$[45] in deaerated MeCN. Typically, a quinoxalinoporphyrin was dissolved in CH_2Cl_2 (5.0×10^{-4} M in 300 μL) containing $(BNA)_2$ (2.5×10^{-4} M) and purged with argon for 10 min. The solution was bubbled with Ar gas through a syringe that has a long needle. ESR spectra were recorded on a JEOL JES-RE1XE spectrometer under irradiation of a high-pressure mercury lamp (USH-1005D) by focusing at the sample cell in the ESR cavity at 298 K. The magnitude of modulation was chosen to optimize the resolution and signal-to-noise ratio of

the observed spectra under nonsaturating microwave power conditions. The *g* values were calibrated using a Mn^{2+} marker.

Calculations. Calculations of the properties of molecules were performed using DFT with the B3LYP density functional[49] and the 6-31G(d) basis set. All calculations were performed using Gaussian 03.[50] Graphical outputs of the computational results were generated with the Gaussview software program (version 3.09) developed by Semichem, Inc.[51] The hyperfine coupling constants were determined by computer simulation using the Calleo ESR program (version 1.2) coded by Calleo Scientific on a personal computer.

Acknowledgment. The support of the Robert A. Welch Foundation (K.M.K., Grant No. E-680) and the Texas Advanced Research program to K.M.K. under Grant No. 003652-0018-2001 are gratefully acknowledged. This work was also partially supported by a Discovery Research Grant (Grant No. DP0208776) to M.J.C. and J.R.R. from the Australian Research Council and a Grant-in-Aid (Grant No. 19205019) to S.F. from the Ministry of Education, Culture, Sports, Science and Technology, Japan. We thank the Australian Partnership for Advanced Computing for provision of the computational resources.

References and Notes

(1) Kim, D.; Osuka, A. *Acc. Chem. Res.* **2004**, *37*, 735.

(2) Fukuzumi, S.; Imahori, H. In *Electron Transfer in Chemistry*; Balzani V. Ed.; Wiley-VCH: Weinheim, Germany, 2001; Vol. 2, pp 927−975.

(3) Holten, D.; Bocian, D. F.; Lindsey, J. S. *Acc. Chem. Res.* **2002**, *35*, 57.

(4) Reimers, J. R.; Hush, N. S.; Crossley, M. J. *J. Porphyrins Phthalocyanines* **2002**, *6*, 795.

(5) Jiao, J.; Anariba, F.; Tiznado, H.; Schmidt, I.; Lindsey, J. S.; Zera, F.; Bocian, D. F. *J. Am. Chem. Soc.* **2006**, *128*, 6965.

(6) Kelley, R. F.; Shin, W. S.; Rybtchinski, B.; Sinks, L. E.; Wasielewski, M. R. *J. Am. Chem. Soc.* **2007**, *129*, 3173.

(7) McDermott, G.; Prince, S. M.; Freer, A. A.; Hawthornthwaite-Lawless, A. M.; Papiz, M. Z.; Cogdell, R. J.; Isaacs, N. W. *Nature* **1995**, *374*, 517.

(8) Pullerits, T.; Sundstrom, V. *Acc. Chem. Res.* **1999**, *29*, 381.

(9) (a) Babcock, G. T.; Wikström, M. *Nature* **1992**, *356*, 301. (b) Babcock, G. T. *Proc. Natl. Acad. Sci. U.S.A.* **1999**, *96*, 12971.

(10) Blankenship, R. E. *Molecular Mechanisms of Photosynthesis*; Blackwell Science: Oxford, U. K., 2002.

(11) Wasielewski, M. R. *J. Org. Chem.* **2006**, *71*, 5051.

(12) Crossley, M. J.; Sintic, P. J.; Hutchison, J. A.; Ghiggino, K. P. *Org. Biomol. Chem.* **2005**, *3*, 852.

(13) (a) Lindsey, J. S., In *The Porphyrin Handbook*; Kadish, K. M., Smith, K. M., Guilard, R., Eds.; Academic Press: San Diego, 2000; Vol. 1, pp 45−118. (b) Jaquinod, L., In *The Porphyrin Handbook*; Kadish, K. M., Smith, K. M., Guilard, R., Eds.; Academic Press: San Diego, 2000; Vol. 1, pp 201−237.

(14) (a) Burrell, A. K.; Officer, D. L.; Plieger, P. G.; Reid, D. C. W. *Chem. Rev.* **2001**, *101*, 2751. (b) Bonfantini, E. E.; Burrell, A. K.; Campbell, W. M.; Crossley, M. J.; Gosper, J. J.; Harding, M. M.; Officer, D. L.; Reid, D. C. W. *J. Porphyrins Phthalocyanines* **2002**, *6*, 708.

(15) Osuka, A.; Shimidzu, H. *Angew. Chem., Int. Ed.* **1997**, *109*, 135.

(16) (a) Crossley, M. J.; Burn, P. L. *J. Chem. Soc., Chem. Commun.* **1987**, 39. (b) Crossley, M. J.; McDonald, J. A. *J. Chem. Soc., Perkin Trans. 1* **1999**, 2429.

(17) (a) Siri, O.; Jaquinod, L.; Smith, K. M. *Tetrahedron Lett.* **2000**, *41*, 3583. (b) Shea, K. M.; Jaquinod, L.; Khoury, R. G.; Smith, K. M. *Tetrahedron* **2000**, *56*, 3139.

(18) (a) Kim, D.; Osuka, A. *J. Phys. Chem. A* **2003**, *107*, 8791. (b) Cho, H.; Jeong, D. H.; Cho, S.; Kim, D.; Matsuzaki, Y.; Tanaka, K.; Ysuda, A.; Osuka, A. *J. Am. Chem. Soc.* **2002**, *124*, 14642.

(19) Nakamura, Y.; Aratani, N.; Shinokubo, H.; Takagi, A.; Kawai, T.; Matsumoto, T.; Yoon, Z. S.; Kim, D. Y.; Ahn, T. K.; Kim, D.; Muranaka, A.; Kobayashi, N.; Osuka, A. *J. Am. Chem. Soc.* **2006**, *128*, 4119.

(20) Crossley, M. J.; Burn, P. L. *J. Chem. Soc., Chem. Commun.* **1991**, 1569.

(21) Anderson, H. L. *Inorg. Chem.* **1994**, *33*, 972.

(22) Tsuda, A.; Osuka, A. *Science* **2001**, *293*, 79.

(23) Fletcher, J. T.; Therien, M. J. *Inorg. Chem.* **2002**, *41*, 331.

(24) Sendt, K.; Johnston, L. A.; Hough, W. A.; Crossley, M. J.; Hush. N. S.; Reimers, J. R. *J. Am. Chem. Soc.* **2002**, *124*, 9299.

(25) Li, F.; Yang, S. I.; Ciringh, Y.; Seth, J.; Martin, C. H., III.; Singh, D. L.; Kim, D.; Birge, R. R.; Bocian, D. F.; Holten, D.; Lindsey, J. S. *J. Am. Chem. Soc.* **1998**, *120*, 10001.

(26) Lammi, R. K.; Wagner, R. W.; Ambroise, A.; Diers, J. R.; Bocian, D. F.; Holten, D.; Lindsey, J. S. *J. Phys. Chem. B* **2001**, *105*, 5341.

(27) Crossley, M. J.; Govenlock, L. J.; Prashar, J. K. *J. Chem. Soc., Chem. Commun.* **1995**, 2379.

(28) Reimers, J. R.; Lu, T. X.; Crossley, M. J.; Hush, N. S. *Nanotechnology* **1996**, *7*, 424.

(29) Metzger, R. M. *Chem. Rev.* **2003**, *103*, 3803.

(30) Reimers, J. R.; Hall, L. E.; Crossley, M. J.; Hush, N. S. *J. Phys. Chem. A* **1999**, *103*, 4385.

(31) Kadish, K. M.; E, W.; Zhan, R.; Khoury, T.; Govenlock, L. J.; Prashar, J. K.; Sintic, P.; Ohkubo, K.; Fukuzumi, S.; Crossley, M. J. *J. Am. Chem. Soc.* **2007**, *129*, 6576.

(32) Crossley, M. J.; Sintic, P. J.; Walton, R.; Reimers, J. R. *Org. Biomol. Chem.* **2003**, *1*, 2777.

(33) Yeow, E. K. L.; Sintic, P. J.; Cabral, N. M.; Reek, J. N. H.; Crossley, M. J.; Ghiggino, K. P. *Phys. Chem. Chem. Phys.* **2000**, *2*, 4281.

(34) (a) Crossley, M. J.; Harding, M. M.; Sternhell, S. *J. Am. Chem. Soc.* **1986**, *108*, 3608. (b) Crossley, M. J.; Field, L. D.; Harding, M. M.; Sternhell, S. *J. Am. Chem. Soc.* **1987**, *109*, 2335. (c) Crossley, M. J.; Harding, M. M.; Sternhell, S. *J. Org. Chem.* **1988**, *53*, 1132. (b) Crossley, M. J.; Harding, M. M.; Sternhell, S. *J. Org. Chem.* **1992**, *57*, 1833.

(35) Seely, G. R. *J. Chem. Phys.* **1957**, *27*, 125.

(36) Gouterman, M., In *The Porphyrins*; Dolphin, D., Ed. Academic Press: New York, 1978; Vol. 3, pp 16−19.

(37) Crossley, M. J.; Harding, M. M.; Sternhell, S. *J. Am. Chem. Soc.* **1992**, *114*, 3266.

(38) Ou, Z.; E, W.; Shao, J.; Burn, P. L.; Sheehan, C. S.; Walton, R.; Kadish, K. M.; Crossley, M. J. *J. Porphyrins Phthalocyanines* **2005**, *9*, 142.

(39) Kadish, K. M.; Lin, M.; Caemelbecke, E. V.; Stefano, G. D.; Medforth, C. J.; Nurco, D. J.; Nelson, N. Y.; Krattinger, B.; Muzzi, C. M.; Jaquinod, L.; Xu, Y.; Shyr, D. C.; Smith, K. M.; Shelnutt, J. A. *Inorg. Chem.* **2002**, 6673.

(40) Kadish, K. M.; Van-Caemelbecke, E.; Royal, G., In *The Porphyrin Handbook*; Kadish, K. M., Smith, K. M., Guilard, R., Eds.; Academic Press: San Diego, 2000; Vol. 8, pp 1−114.

(41) The one-electron reduction of $(PQ_2)Cu$ also results in a similar spectral change to that of (PQ)Cu. However, the long-wavelength absorption becomes broader as compared to that of (PQ)Cu.

(42) The absorption spectrum of the radical cation of (QPQ)Cu is similar to that of (PQ)Cu.

(43) Patz, M.; Kuwahara, Y.; Suenobu, T.; Fukuzumi, S. *Chem. Lett.* **1997**, 567.

(44) Fukuzumi, S.; Suenobu, T.; Patz, M.; Hirasaka, T.; Itoh, S.; Fujitsuka, M.; Ito, O. *J. Am. Chem. Soc.* **1998**, *120*, 8060.

(45) Some disagreement between the observed hyperfine coupling constants and calculated spin densities may also result from the effects of solvation and the ion pair formation with the counter cation (BNA^+).

(46) Aviram, A.; Ratner, M. A. *Chem. Phys. Lett.* **1974**, *29*, 277.

(47) Crossley, M. J.; Prashar, J. K. *Tetrahedron Lett.* **1997**, *38*, 6751.

(48) Reimers, J. R.; Lü, T. X.; Crossley, M. J.; Hush, N. S. *Nanotechnology* **1996**, *7*, 424.

(49) Becke, A. D. *J. Chem. Phys.* **1993**, *98*, 5648.

(50) Frisch, M. J.; Trucks, G. W.; Schlegel, H. B.; Scuseria, G. E.; Robb, M. A.; Cheeseman, J. R.; Montgomery, J. A., Jr.; Vreven, T.; Kudin, K. N.; Burant, J. C.; Millam, J. M.; Iyengar, S. S.; Tomasi, J.; Barone, V.; Mennucci, B.; Cossi, M.; Scalmani, G.; Rega, N.; Petersson, G. A.; Nakatsuji, H.; Hada, M.; Ehara, M.; Toyota, K.; Fukuda, R.; Hasegawa, J.; Ishida, M.; Nakajima, T.; Honda, Y.; Kitao, O.; Nakai, H.; Klene, M.; Li, X.; Knox, J. E.; Hratchian, H. P.; Cross, J. B.; Bakken, V.; Adamo, C.; Jaramillo, J.; Gomperts, R.; Stratmann, R. E.; Yazyev, O.; Austin, A. J.; Cammi, R.; Pomelli, C.; Ochterski, J. W.; Ayala, P. Y.; Morokuma, K.; Voth, G. A.; Salvador, P.; Dannenberg, J. J.; Zakrzewski, V. G.; Dapprich, S.; Daniels, A. D.; Strain, M. C.; Farkas, O.; Malick, D. K.; Rabuck, A. D.; Raghavachari, K.; Foresman, J. B.; Ortiz, J. V.; Cui, Q.; Baboul, A. G.; Clifford, S.; Cioslowski, J.; Stefanov, B. B.; Liu, G.; Liashenko, A.; Piskorz, P.; Komaromi, I.; Martin, R. L.; Fox, D. J.; Keith, T.; Al-Laham, M. A.; Peng, C. Y.; Nanayakkara, A.; Challacombe, M.; Gill, P. M. W.; Johnson, B.; Chen, W.; Wong, M. W.; Gonzalez, C.; Pople, J. A. *Gaussian 03*, revision C.02; Gaussian, Inc.: Wallingford, CT, 2004.

(51) Dennington, R., II.; Keith, T.; Millam, J.; Eppinnett, K.; Hovell, W. L.; Gilliland, R. *Gaussview*; Semichem, Inc.: Shawnee Mission, KS, 2003.